**MinEx CRC Limited**
26 Dick Perry Avenue, Kensington, WA, 6151
PO Box 1130, Bentley, WA, 6102, Australia
admin@minexcrc.com.au

ABN: 66 625 533 913

**MinEx CRC provides financial support to the value of $1K to promote Honours and Masters by Coursework projects that are aligned with the mission of MinEx CRC and to encourage young researchers toward a career in mineral exploration research. Projects are not restricted to MinEx CRC Participants and Affiliates.**

**Please note that the content of this thesis has not been subjected to peer-review and subsequent corrections.**

Australian Government
Department of Industry, Science and Resources
Cooperative Research Centres Program

# Mining and mineral processing
# A mineralogical and geochemical toolkit for ore deposit targeting

**by**

**Zhaolin Hao**

**Supervisor: Dr. Sudeshna Basugupta**

**September 2022**

**A thesis submitted to the University College London for the degree of Master of Science (MSc) in Global Management of Natural Resources**

**Department of Chemical Engineering**

**University College London**

**In collaboration with**

**Future Industries Institute**

**University of South Australia**

# ABSTRACT

Copper is a key metal in human society, and the demand for copper has been increasing. Porphyry copper deposits and IOCG deposits are the main sources of copper, gold, and other important metals. However, because most of the surface deposits have been discovered, new technologies need to be developed to find unknown deposits buried underground. Zircon geochemistry provides a great opportunity to develop new tools for copper exploration. This study collects and collates the zircon geochemical data from all over the world, and plots these data on the zircon geochemical criteria developed by Brotodewo et al. (2021) and Lu et al. (2016) for IOCG deposits and porphyry deposits, respectively. The results verify that zircon chemistry can generally be used as the indicator for porphyry deposits, and can identify the background zircon and IOCG zircon in South Australia, but cannot effectively distinguish other IOCG deposits.

Keywords: zircon; geochemistry; IOCG deposits; porphyry deposits; mineral exploration

# CONTENTS

# List of Figures and Tables

# 1. INTRODUCTION

Copper is a key metal for electric vehicles, wind and solar energy, and infrastructure for transporting and storing renewable energy (Stevens, 2022). The energy transformation has pushed the demand for copper to an unprecedented level (Stevens, 2022). However, the replacement and recovery of copper are insufficient to meet the demand for electric vehicles (EVS), power infrastructure, and renewable energy suppliers (Greenhalgh, 2022). The total demand for copper will nearly double from just over 25 million tons (MT) in 2021 to nearly 49 million tons in 2035, and then reach 53 million tons in 2050(Greenhalgh, 2022).

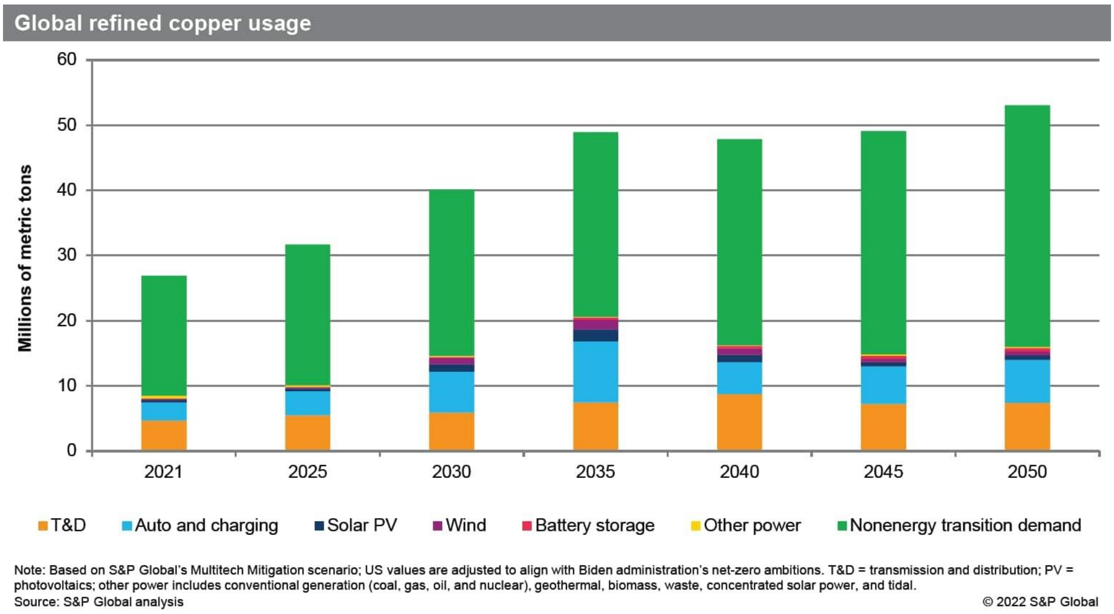


*Figure 1:  The Future demand of Copper (S&P Global, 2022)*

In order to meet the growing demand for metals, explorers need to discover more new deposits. However, most surface deposits have been discovered and exploited, and exploration needs to be carried out in the regions covered by the deposits (Brotodewo et al., 2021). Therefore, new technologies are needed to locate these covered deposits, reduce costs, and improve the success rate of mineral discovery (Forbes et al., 2015). In particular, the geochemistry of cover rock sequences overlying mineralised basement rocks has proven to be very useful in mineral exploration, although they were considered obstacles to exploration in the past (Brotodewo et al., 2021).

Zircon is a typical accessory mineral found in igneous rocks, because of its strong physical and chemical stability (Bao et al., 2014), it is widely used in the field of petrology and geochemistry. Zircon geochemistry has recently been proved to be a useful indicator for mineral exploration. The use of zircon chemistry as an indicator of ore-forming fertility and as a possible exploration tool for the discovery of underground porphyry deposits (Lu et al., 2016) and IOCG deposits (Brotodewo et al., 2021) have been confirmed. For porphyry deposits, zircons in fertile intrusive rocks have more obvious Eu anomalies and Ce anomalies than those in infertile intrusive rocks (Lu et al., 2016). The research of Brotodewo et al. (2021) shows that the Eu anomaly and heavy rare earth element concentration of zircon geochemistry are related to the magmatic fertility of the volcanic rocks in the IOCG mining area, but this study was only carried out in the Gawler Craton, South Australia, so the significance of this correlation is still under further study.

This study collects and collates the zircon data of six publications from different deposits around the world, and plots these data on the zircon geochemical criteria developed by Brotodewo et al. (2021) and Lu et al. (2016) for IOCG deposits and porphyry deposits respectively. Evaluate the applicability of IOCG zircon geochemical exploration criteria outside the Gawler Craton in South Australia by checking whether the background zircon and the zircon data in the mineralised area overlap and look for any similarities or differences between the same global zircon chemical data in the porphyry geochemical exploration criteria plot.

# 2. BACKGROUND

## 2.1 Zircon

Zircon is a sodium silicate mineral and its chemical name is zirconium silicate (Zaman and Antao, 2020). The ideal chemical formula of zircon is $ZrSiO_4$ (Zaman and Antao, 2020). Zircon and its derivatives are widely used in human life (ZIRCON INDUSTRY ASSOCIATION， 2022). Ground zircon is characterised by its high hardness, whiteness, and opacity, which allows zircon to be used as a sunscreen in ceramics (Eramet, 2020). Zircon also has the characteristics of high-temperature resistance and acid corrosion resistance (Eramet, 2020). The melting point of zircon is 2750℃ (Römer, Luther and Assmus, 1994), which makes zircon very suitable for casting and refractories (Eramet, 2020). The abrasion resistance and diamond-like luster of zircon make it a popular material in jewelry(ZIRCON INDUSTRY ASSOCIATION，2022).

## 2.2 Application of zircon in geology

Zircon is a significant mineral in the study of petrology, geochemistry, and chronology (Ghasemi Siani et al., 2022). Zircon has become a vital dating medium for geologists (Ghasemi Siani et al., 2022). One of the widely used methods in geochronology is the technique of radiometric dating based on (U-Pb) radioactive decay, the most commonly used mineral in this method being zircon (Bao et al., 2014). With the passage of time, the zircon contains a small amount of uranium and thorium which will undergo radioactive decay (American Museum of Natural History, 2019). Since the rate of radioactive decay is known, scientists can measure the trace amounts of these elements in zircon to determine the age of the host rock (Hazen, 2010). Their oxygen isotope ratios preserve the original δ18O record, so measuring the oxygen isotopes of ancient zircon can indicate the origin and genesis of the rocks and help explore crustal-hydrosphere interactions billions of years ago (Mojzsis, Harrison and Pidgeon, 2001). Measuring the Ti content of zircon can estimate crystallization temperatures and infer crystallization conditions (Fu et al., 2008). In addition, the extremely low diffusivity of most elements in zircons allows for zoning of trace element content and is considered to record major features during zircon formation or reprecipitation, even during subsequent high-grade metamorphism (Roberts, Yang and Santosh, 2018). Finally, the rare earth elements in zircon can help determine the growth time of zircon and other minerals relative to each other (Spencer，2012). For example, when zircon is grown in the presence of garnet, which consumes more rare earth elements than zircon, and when zircon is grown without garnet, the concentration of rare earth elements in zircon is much higher (Spencer，2012).

## 2.3 Formation environment of zircon

Three types of zircon can be naturally formed: magmatic, metamorphic, and hydrothermal (Yang et al., 2013). Magmatic zircon crystallizes from magma (e.g. granitic magma) (Yang et al., 2013). This type of zircon will have oscillatory zones and abundant melt and mineral inclusions (Yang et al., 2013). Metamorphic zircon forms due to changes in pressure and at temperatures of more than 900°C (Bao et al., 2014). The zircon is chemically stable at a temperature of at least 900°C (Yang et al., 2013). Hydrothermal zircon crystallises from or is altered by hydrothermal fluids (Yang et al., 2013). The temperature of hydrothermal zircon formation ranges from 600°C in the late magmatic system of the magmatic-hydrothermal transition period to 300°C in the hydrothermal mineralisation systems (Bro, 2018; Schaltegger, 2007). Late magmatic-hydrothermal zircons may be precipitated from fluid saturated magma, or from the exsolution fluid of mineralised granite and pegmatite (Schaltegger, 2007).

## 2.4 Chemical composition of zircon for mineral exploration

The hydrothermal properties and isotopic characteristics of zircon particles indicate the influence of hydrothermal solution on mineralisation, and the high-temperature magmatic fluid related to the intrusion is the most likely heat source and fluid source (Westhues et al., 2017). Many studies on known deposits in the world have investigated the geochemical characteristics of zircon and the geochemical trend of hydrothermal zircon (Brotodewo et al., 2018). These studies emphasize the features in hydrothermal zircons, such as unique textures (such as spongy textures formed by fluid inclusions), high REE concentrations, positive Ce anomalies, and negative Eu anomalies (Brotodewo et al., 2018). These studies show that there are obvious geochemical anomalies in hydrothermal zircon compared with igneous zircon or metamorphic zircon (Brotodewo et al., 2018). The geochemical trends of hydrothermal zircon in different places are quite different. This difference can be used as a potentially useful tool for exploring mineral deposits and may be amplified by minerals in these rocks (Li, Watanabe and Yonezu, 2014).

Lu et al. (2016) discussed the potential of zircon as indicators of mineralisation in porphyry Cu ± Mo ± Au systems by distinguishing the geochemical anomalies present in zircon from porphyry-fertile intrusions from those unrelated to porphyry mineralisation. Eu/Eu* (>0.3) and 10,000*(Eu/Eu*)/Y (>1) are considered to be characteristic of magmatic zircon within mineralised zones, and this signature can be used to distinguish between porphyry systems with high and low mineralisation potential（Lu et al., 2016).

Zircon geochemistry is also being researched for IOCG deposits. Brotodewo et al. (2021) used zircon chemistry by analysing detrital zircon grains in the Gawler Craton region of South Australia to assess zircon compositions as an important exploration tool for IOCG deposits. Brotodewo et al. (2018, 2021) showed that the unique geochemical characteristics of zircon, such as texture, high rare earth element (REE) concentrations, positive Ce anomalies, and negative Eu anomalies, make them indicators of magmatic fertility and mineralisation (Brotodewo et al., 2018). However, this study was only conducted at the Gawler Craton in South Australia, and research is ongoing as to whether this criterion can be used to explore IOCG deposits elsewhere in the world (Brotodewo et al., 2021).

## 2.5 Cu-Au mineral deposits

### *2.5.1 Iron oxide-copper gold deposits*

IOCG deposits are one of the most important sources of copper, gold, and critical commodities (Del Real et al., 2021).  IOCG deposits are characterised by large scale, relatively simple metallurgy, and relatively high grades for highly profitable mining operations (Schlegel, Wagner and Fusswinkel, 2020; Real et al., 2021). The IOCG ore deposit contains between 10 million and 4 billion tonnes of ore, with a copper grade of 0.2% to 5% and a gold concentration of between 0.1 and 3+ grams per tonne  (Hitzman, Oreskes and Einaudi, 1992). The gold content in these deposits varies greatly, which may be a factor affecting the economic value of the deposits. IOCG deposits may also contain high levels of light rare earth elements (LREE), silver, molybdenum, nickel, cobalt, barium, fluorine, and phosphorus, which are by-product strategic elements that increase their attractiveness, although these attachments are generally less economical than copper and gold (Del Real et al., 2021). The ore minerals of IOCG deposit are usually copper iron sulfide chalcopyrite and gangue pyrite, accounting for 10-15% of the rock mass (Encyclopedia Britannica, 2022).

IOCG deposits formed through magmatic and hydrothermal activity (Groves et al., 2010). The creation of IOCG deposits is linked to deep fracture tectonics and large-scale magmatic activity (Del Real et al., 2021). The former offers a route for volcanic magma and related fluids to up well, while the latter provides the driving force and material source for mineralizing fluids to circulate convectively (Skirrow, 2021). A water-rock effect occurs when magmatic-hydrothermal fluids are combined with at least one other fluid, resulting in mineralised component enrichment (Skirrow, 2021). Models of non-magmatic diagenesis published in the literature show that the origins of metals, fluids, ligands, and sulfur are all still a mystery (Schlegel, Wagner and Fusswinkel, 2020). The wide variability between IOCG deposits is one of their distinguishing features. The lack of a complete model characterising deposit development is due to differences in ore grade, alteration style, and fluid inclusions, and no generalised deposit model can describe the variability of IOCG deposits on a worldwide basis (WILLIAMS, 2001).

The continental margin extensional zone and continental rift zone are the most common locations of IOCG deposits (Skirrow, 2021). The IOCG deposit also has strong tectonic control and is not closely related to igneous rocks in time but in space (Zhu, 2016). Figure 2 shows the 11 IOCG provinces in the strict sense.

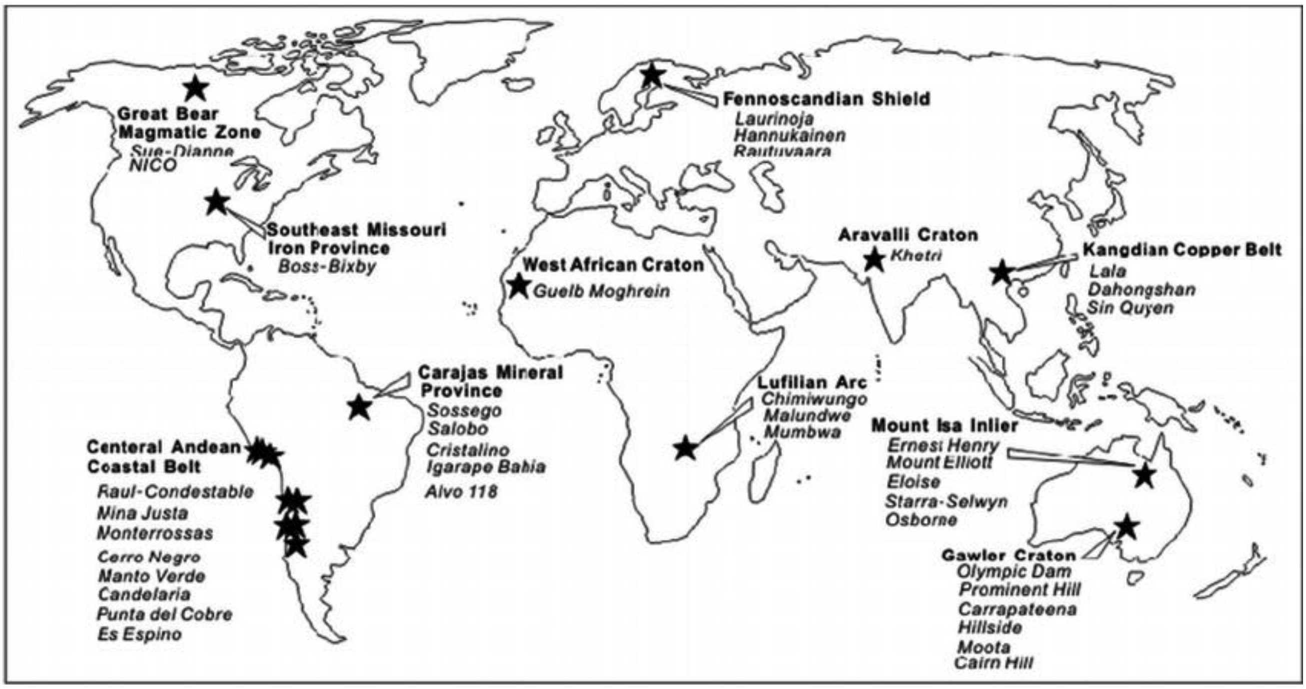


*Figure 2: IOCG deposits distribution map (Zhu, 2016)*

### *2.5.2 Porphyry copper deposits*

Porphyry copper deposits are the natural suppliers of most copper and important gold in our society (Chiaradia, 2020). Porphyry deposits produce over 70% of the world's copper and about 20% of the world's gold, of which gold is the most valuable metal, accounting for about 25% of the deposits (Dilles and John, 2021). Large deposits and low grades define porphyry copper deposits (Chiaradia, 2020**)**. Porphyry copper deposits usually contain hundreds of millions of tons of ore, with an average copper content of 1% by weight (Encyclopedia Britannica, 2022). Despite their low grade, porphyry deposits can be exploited on a large scale at a low cost (Encyclopedia Britannica, 2022). In addition, rhenium, platinum group elements (PGE), bismuth, and tellurium, as well as a large amount of silver and zinc, are produced as by-products (Dilles and John, 2021).

Porphyry copper deposits are magmatic-hydrothermal mineralisation systems (Alizadeh Sevari and Hezarkhani, 2014). The upper mantle/lower crust provides the metallogenic hydrothermal fluid for porphyry copper ore (Dilles and John, 2021). Due to variations in temperature and pressure, the ore mass and mineralizing hydrothermal fluid are exsolved by magma during upward intrusion and crystallisation after intrusion and are enriched in ideal mineralisation regions (Dilles and John, 2021). Porphyry copper deposits formed in an environment of plate subduction, collision, and tension (Richards, 2009). The majority of porphyry copper deposits are related to the Andean subduction zone calc-alkaline magmas (Chiaradia, 2020).

Porphyry copper deposits are one of the metal deposits genetically related to plate activity (Dilles and John, 2021). The porphyry copper deposits seem to coincide with the orogenic belt (Sillitoe, 2010). This significant association is most obvious in the Mesozoic to Cenozoic sediments of the circum Pacific Ocean, but also in the Paleozoic sediments of North America, Australia, and the Soviet Union within the orogenic belt (Sillitoe, 2010). Porphyry deposits occur in two main environments within the orogenic belt - in the island arc and continental margin (Oliveira et al., 2016). Cenozoic and, to a lesser extent, Mesozoic sediments dominate  (Oliveira et al., 2016). Most of the known porphyry copper deposits are concentrated in Western North and South America and Southeast Asia and Oceania along the Pacific Ring of fire; the southern part of central Europe; China, the Middle East, and Russia; eastern Australia (Sillitoe, 2010). Figure 3 shows the distribution of porphyry copper deposits in the world.

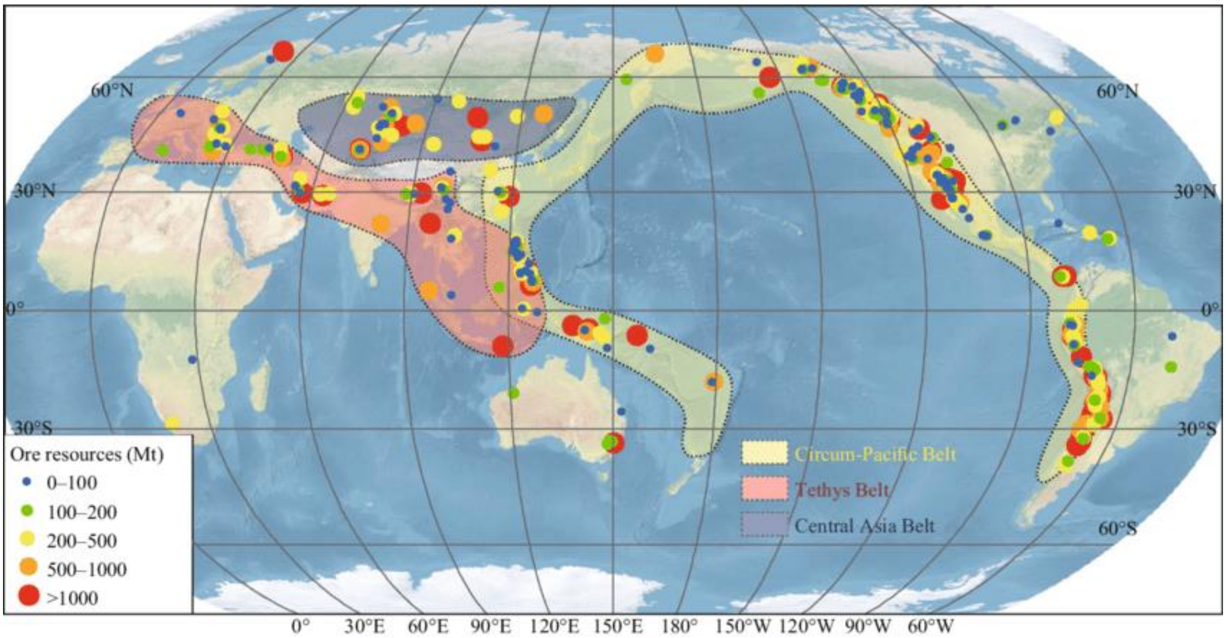


*Figure 3: Porphyry copper deposits distribution map (Liu et al., 2019)*

# 3. METHODOLOGY

## 3.1 Collating data from the literature

This study collates zircon data sets from six publications. Three publications are about IOCG deposits (Brotodewo et al., 2021; Fuentes-Guzmán et al., 2020; Li et al., 2015) and the other three are about Porphyry deposits (Lu et al., 2016; Zheng et al., 2021; Pizarro et al., 2020). Among them, Brotodewo et al. (2021) and Lu et al. (2016) developed geochemical exploration criteria for IOCG and porphyry deposits respectively. Data from the other four articles are plotted and compared with these geochemical exploration criteria. The regions of the chemical composition of zircons evaluated in the six publications are the Lamandau IOCG deposit in Indonesia, the IOCG skarn deposits in central and eastern Mexico, the Carrapateena IOCG deposit in South Australia, the porphyry gold deposit in Southwest China, the porphyry copper deposits in Northern Chile (Fuentes-Guzmán et al., 2020, Zheng et al., 2021, Li et al., 2015, Pizarro et al., 2020), and a series infertile suites and fertile suites around the world collected from Lu et al. (2016).

## 3.2 Sample preparation

In the literature, the authors collect zircon data through three steps; preparing the samples, analyzing the internal structures, and collection of elemental data. The first step is to prepare samples. Zircons were hand-picked under a binocular microscope after being extracted from samples using magnetic and heavy liquid separation techniques (Brotodewo et al., 2021, Li et al.,2015). Zircon particles were then adhered to tape, covered in epoxy, polished to a thickness of roughly half, and covered in carbon (Brotodewo et al., 2021, Li et al.,2015). When choosing samples, care was taken to avoid prejudice and to choose a variety of sizes, colours, and shapes (Brotodewo et al., 2021, Lu et al, 2016).

## 3.3 Analyse zircon for internal texture

The second step is to analyze the internal structure of the zircon using the Scanning Electron Microscope (SEM) using cathodoluminescence imaging (CL imaging). Using the internal texture characterisation capabilities of the MLA quanta SEM 600, the morphology and internal structure of zircon grains were photographed under cathodoluminescence (CL) (Brotodewo et al., 2021).

## 3.4 Collecting data

The third step is to collect geochemical data. Laser ablation inductively coupled mass spectrometry (LA-ICP-MS) is used to collect rare earth elements and trace element geochemistry (Brotodewo et al., 2021). Data were processed using the software 'Iolite', two silicate glass reference materials (NIST SRM610, NIST SRM612) to correct for mass bias drift during the analysis (Brotodewo et al., 2021, Pizarro et al.,2020). Calibration was also completed using internal standards and matrix normalization.

Data from literature was used to calculate Eu/Eu*, 10,000*(Eu/Eu*)/Y, Ce/Nd, (Ce/Nd)/Y, Dy/Yb, and HREE Frac to test whether the discrimination plots by Brotodewo et al. (2021) & Lu et al. (2016) were applicable in other regions. All collected zircon data were normalized to Taylor & McLennan (1985).

# 4. RESULTS

## 4.1 Samples summary

Table 1 & 2 provides a summary of samples used in this study, including sample ID, location, country, age, deposit type, and comments.

Table1: Detail of zircon from fertile suites

| Sample_ID | Location | Country | Age (Ma) | Deposit type | Comments |
|---|---|---|---|---|---|
| R05076A | Batu Hijau | Indonesia | 3.7 | Porphyry Cu-Au deposit | Collated from (Lu et al., 2016), named “Porphyry-fertile” (in the following plots) |
| R05044A | Tampakan | Philippines | 3.8 | Porphyry and high-sulfidation Cu-Au deposit | |
| DT071 | Dexing | China | 170 | Porphyry Cu-Mo-Au deposit | |
| NNH5 | Nannihu | China | 140 | Porphyry Mo deposits | |
| YC083 | Yuchiling | China | 134 | Porphyry Mo deposits | |
| ZK001 | Qulong | China | 16 | Porphyry Cu-Mo deposit | |
| JM5 | Jiama | China | 16 | Porphyry-skarn Cu-Mo-Au deposit | |
| 2013_534 | Sar Cheshmeh | Iran | 13 | Porphyry Cu-Mo-Au deposit | |
| 2015-195 | Sungun | Iran | 21 | Porphyry Cu-Mo deposit | |
| FIA_02/ FIA_03/ FIA_17 FIA_26 | Gawler Craton | Australia | 1600-1570 | IOCG deposit | Collated from (Brotodewo et al., 2021), named “IOCG-Carrapateena” (in the following plots) |
| ES-3 | Escalona | Mexico | 4.11 ± 0.11 | IOCG skarn deposit | Collated from (Fuentes-Guzmán et al., 2020), named “IOCG_Tatatila–Las Minas” (in the following plots) |
| CR-5 | Carboneras | Mexico | 15.05 ± 0.94 | IOCG skarn deposit | |
| 5S-1 | Cinco Señores | Mexico | 15.09 ± 0.48 | IOCG skarn deposit | |
| SC-2b | Santa Cruz | Mexico | 16.34 ± | IOCG skarn deposit | |

| | | | | | |
|---|---|---|---|---|---|
| | | | 0.20 | | |
| BQ-1a | Boquillas | Mexico | 286 ± 2 | IOCG skarn deposit | |
| BQ-1b | Boquillas | Mexico | 13.92 ± 0.22 | IOCG skarn deposit | |
| YA-1 | Yaoan | China | 46 ~ 33 | Porphyry gold deposit | Collated from (Zheng et al., 2021), named "Porphyry-Yaoan" (in the following plots) |
| 11KLLA1/ 11KLLA2/ 11KLLA3 | Southwestern Kalimantan Island | Indonesia | 82.1 ± 1.7 | IOCG deposit | Collated from (Li, Yang and Sun, 2015), named "IOCG Lamandau" (in the following plots) |
| Ch04/ Ch07/ Ch18 | Chuquicamata | Chile | 35.2±0.4 | Porphyry copper deposits | Collated from (Pizarro et al., 2020), named "Porphyry-Chile" (in the following plots) |
| M01/ M03 | Mirador | Chile | 40.6 ± 1.1 | Porphyry copper deposits | |
| Esp03/ Esp01/ | Esperanza | Chile | 41.3 ± 0.3 | Porphyry copper deposits | |
| Esc06/ Esc09/Esc03 | Escondida | Chile | 38-37 | Porphyry copper deposits | |

Table 2: Detail of zircon from infertile suites

| Sample_ID | Location | Country | Age (Ma) | Lithology | Comments |
|---|---|---|---|---|---|
| BT01-BSH10 (485) | Uppermost Plinian fall, Bishop tuff | USA | 0.76 | Rhyolite | Collated from (Lu et al., 2016), named "Porphyry-infertile" (in the following plots) |
| SV51 (486) | Hawkins | Australia | 430 | Dacite | |
| BV-5 (487) | Kadoona | Australia | 414 | Dacite | |
| Y-2 | Mesa Falls tuff, Yellowstone | USA | 1.3 | Fayalite rhyolite | |
| Y-3 | Lava Creek tuff, Yellowstone | USA | 0.64 | Fayalite rhyolite | |
| R05055A | Lucerne pluton | USA | 380 | Granite | |
| NMASH088 (478) | Lower Bandelier plinian fall, Bandelier | USA | 1.5 | Pyroxene rhyolite | |
| NMASH092 (479) | Upper Bandelier plinian fall, Bandelier | USA | 1.1 | Fayalite rhyolite | |
| 2581353/ 2746484/ 2746485/ QGNG | Gawler Craton | Australia | 1850 | Magmatic | Collated from (Brotodewo et al., 2021), named "Background-Donington Suite" (in the following plots) |

| XCY-1 | Yaoan | China | 46 ~ 33 | Quartz syenite porphyry | Collated from (Zheng et al., 2021), named “Yaoan-infertile” (in the following plots) |
|---|---|---|---|---|---|

## 4.2 Calculation results of ratios

Eu/Eu*, 10,000*(Eu/Eu*)/Y, Ce/Nd, (Ce/Nd)/Y, Dy/Yb, and HREE Frac are calculated to reconstruct the zircon chemistry criteria established for IOCG deposits (Brotodewo et al., 2021) and porphyry deposits (Lu et al., 2016).

Table 3 Calculation results of Eu/Eu*, 10,000*(Eu/Eu*)/Y, Ce/Nd, (Ce/Nd)/Y, Dy/Yb, and HREE Frac

| Deposits | | Eu/Eu* | 10,000*(Eu/Eu*)/Y | Ce/Nd | (Ce/Nd)/Y | Dy/Yb | HREE frac |
|---|---|---|---|---|---|---|---|
| IOCG_Tatatila–Las Minas | Range | 0.12-0.91 | 0.44-25.69 | 0.25-47.98 | 0.00003-0.06 | 0.13-1.25 | 0.02-0.56 |
| | Mean | 0.50 | 4.87 | 8.87 | 0.009 | 0.29 | 0.07 |
| | Median | 0.51 | 4.41 | 6.21 | 0.006 | 0.24 | 0.05 |
| IOCG-Lamandau | Range | 0.14-0.69 | The collected data does not contain Y | 6.77-69.48 | - | 0.09-0.27 | 0.01-0.06 |
| | Mean | 0.37 | - | 25.68 | - | 0.20 | 0.04 |
| | Median | 0.37 | - | 22.70 | - | 0.21 | 0.04 |
| IOCG-Carrapateena | Range | 0.05-1.03 | 0.44-15.44 | 0.38-22.61 | 0-0.05 | 0.19-2.24 | 0.02-2.17 |
| | Mean | 0.57 | 2.56 | 3.16 | 0.003 | 0.53 | 0.22 |
| | Median | 0.67 | 2.28 | 1.83 | 0.0007 | 0.49 | 0.16 |
| Background-Donington Suite | Range | 0.05-1.41 | 0.53-8.13 | 0.88-26.25 | 0.0003-0.06 | 0.22-0.78 | 0.03-0.22 |
| | Mean | 0.28 | 2.44 | 6.13 | 0.01 | 0.34 | 0.07 |
| | Median | 0.20 | 1.93 | 4.38 | 0.004 | 0.32 | 0.06 |
| Porphyry-Yaoan | Range | 0.43-0.90 | 4.75-18.87 | 8.06-60.05 | 0.01-0.11 | 0.17-0.25 | 0.03-0.07 |
| | Mean | 0.69 | 10.57 | 20.07 | 0.03 | 0.21 | 0.05 |
| | Median | 0.71 | 10.43 | 14.92 | 0.02 | 0.20 | 0.05 |
| Porphyry-Chile | Range | 0.22-0.94 | 1.44-37.5 | 4.8-143 | 0-4.12 | 0.1-0.3 | 0.01-0.07 |
| | Mean | 0.52 | 8.89 | 52.57 | 0.11 | 0.21 | 0.04 |
| | Median | 0.51 | 7.50 | 22.94 | 0.03 | 0.20 | 0.04 |
| Porphyry-fertile | Range | 0-4.37 | 0-137.35 | 0.34-245.71 | 0.001-0.87 | 0.06-1.06 | 0.01-0.48 |
| | Mean | 0.48 | 8.51 | 22.11 | 0.04 | 0.24 | 0.04 |
| | Median | 0.53 | 7.09 | 15.99 | 0.02 | 0.20 | 0.03 |
| Yaoan-infertile | Range | 0.56-1.05 | 2.8-11.94 | 2.81-8.57 | 0.002-0.01 | 0.31-0.56 | 0.09-0.21 |
| | Mean | 0.75 | 7.48 | 5.47 | 0.01 | 0.40 | 0.13 |

| | | | | | | | |
|---|---|---|---|---|---|---|---|
| | Median | 0.74 | 7.60 | 5.43 | 0.01 | 0.38 | 0.13 |
| Porphyry-infertile | Range | 0.003-0.82 | 0.003-27.94 | 0.34-43.26 | 0.0001-0.12 | 0.12-0.87 | 0.01-0.62 |
| | Mean | 0.16 | 1.65 | 7.25 | 0.007 | 0.33 | 0.07 |
| | Median | 0.09 | 0.51 | 3.60 | 0.002 | 0.32 | 0.06 |

## 4.3 C1 chondrite-normalized REE patterns of zircons

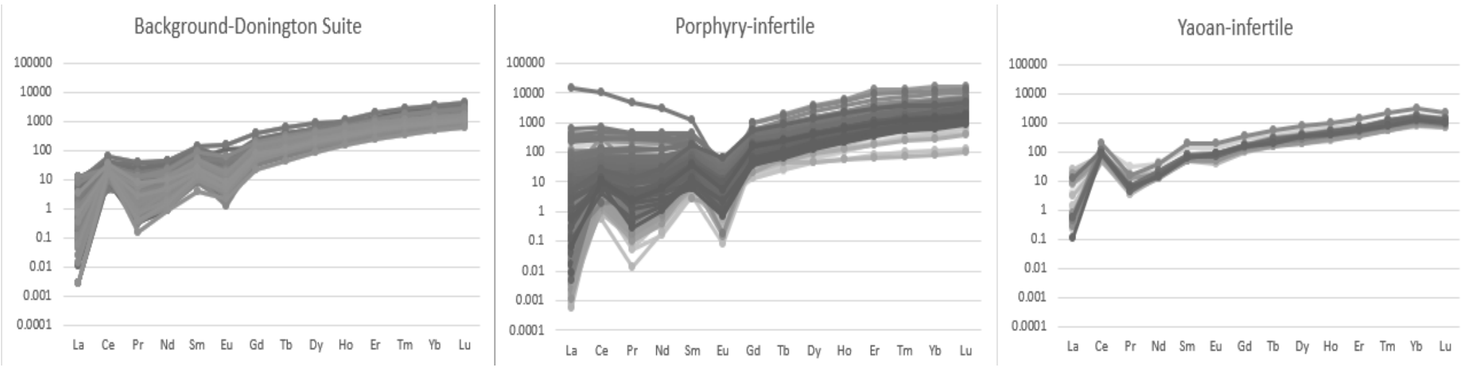


*Figure 4: C1 chondrite-normalized REE patterns of zircons from infertile suites*

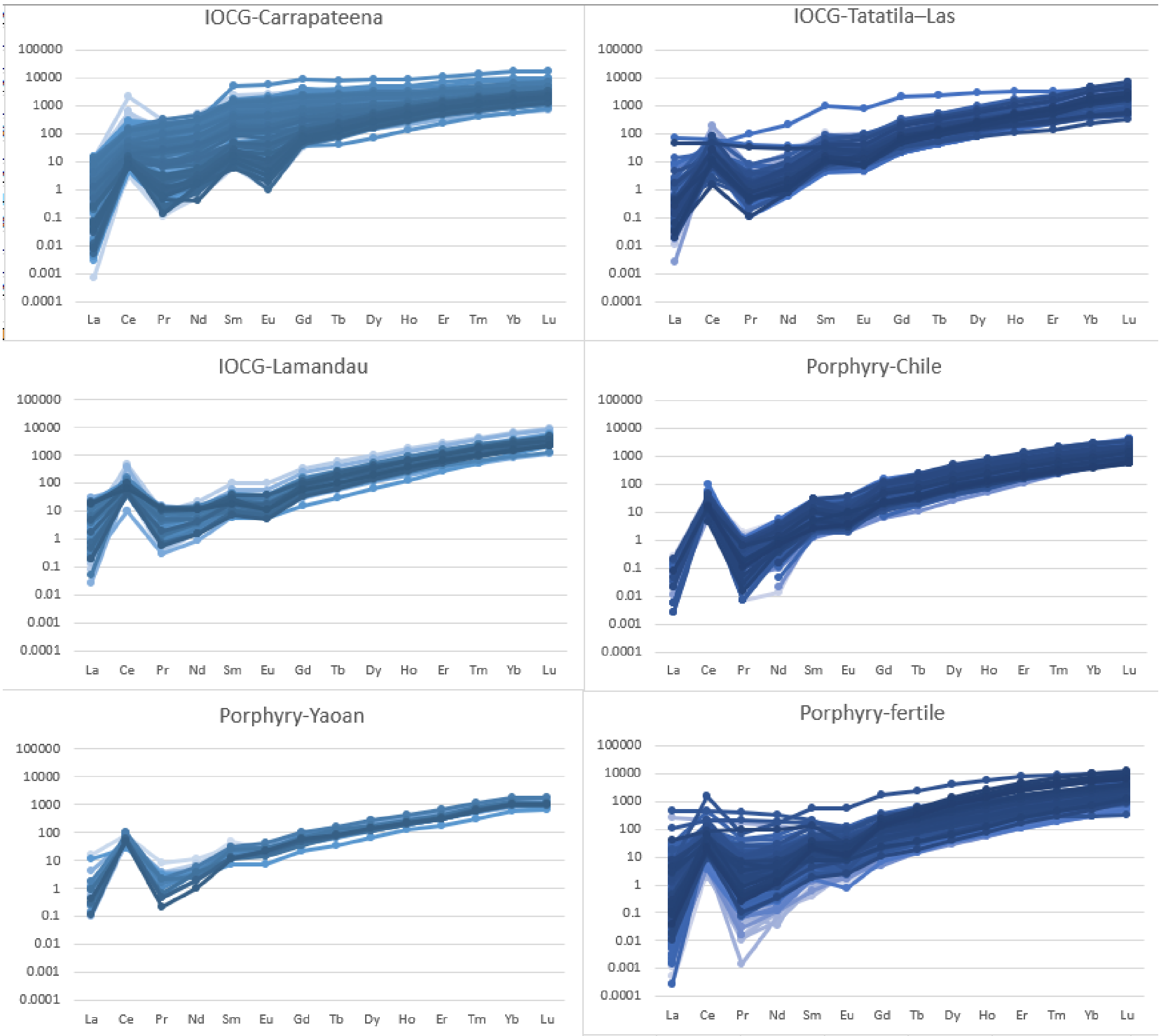


*Figure 5: C1 chondrite-normalized REE patterns of zircons from fertile suites*

Figure 5 shows that zircons from mineralised regions usually have similar overall patterns, characterised by positive Ce and negative Eu anomalies. It is rich in high rare earth elements and lacks light rare earth elements. Compared with non-mineralised intrusions (Fig.4), Ce anomalies are usually larger and Eu anomalies are usually smaller (Fig.5).

### 4.4 Plots of Eu/Eu* vs. Ce/Nd

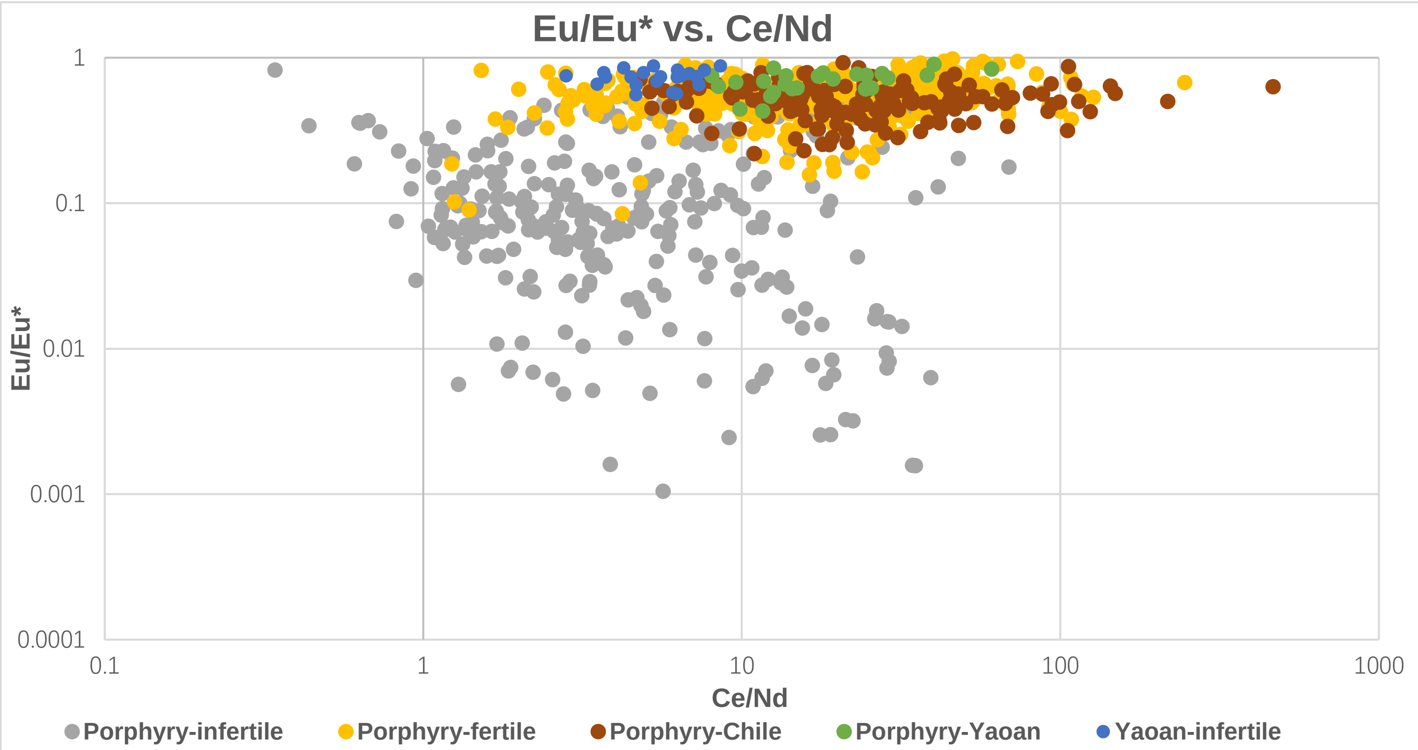


*Figure 6: Zircon Eu/Eu* vs. Ce/Nd plot of porphyry suites and infertile suites*

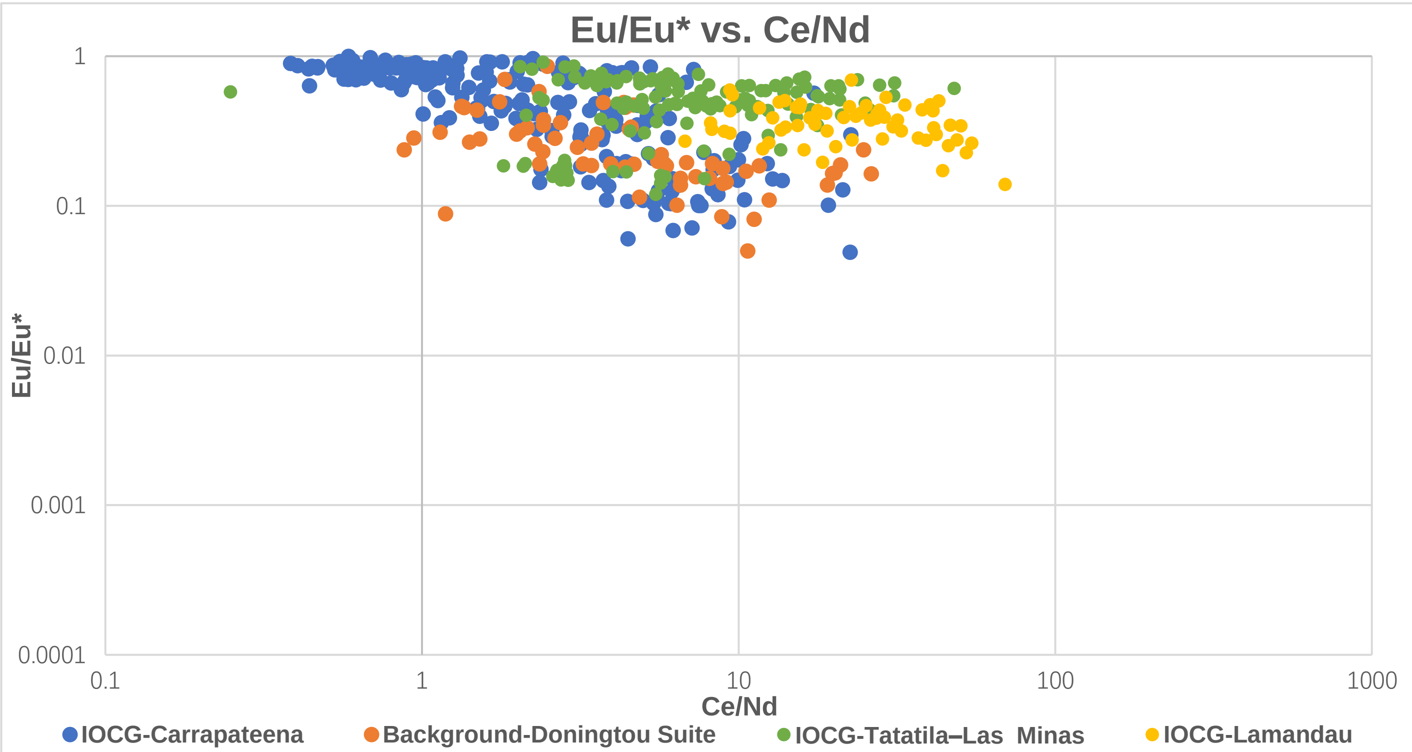


*Figure 7: Zircon Eu/Eu* vs. Ce/Nd plot of IOCG suites and infertile suite*

Figure 6 shows that the zircon Eu/Eu* values of the porphyry suites are significantly higher than those of the infertile suites (>0.3), except for the Yaoan-infertile. The porphyry suites and Porphyry-infertile are separated mainly by the high Eu/Eu* of the fertile suite. The Eu/Eu* of the Porphyry-infertile decreases with increasing Ce/Nd ratios, whereas the Eu/Eu* of the fertile sets and the Yaoan-infertile generally remain constant with increasing Ce/Nd.

Figure 7 shows that IOCG zircon and background zircon are not completely separated. The Eu/Eu* of Background-Donington Suite decreased with increasing Ce/Nd, while IOCG-Carrapateena and IOCG-Lamandau showed a more pronounced tendency to decrease, but the Eu/Eu* of IOCG-Tatatila Las Minas remained constant with increasing Ce/Nd.

### 4.5 Plots of Eu/Eu* vs. (Ce/Nd)/Y

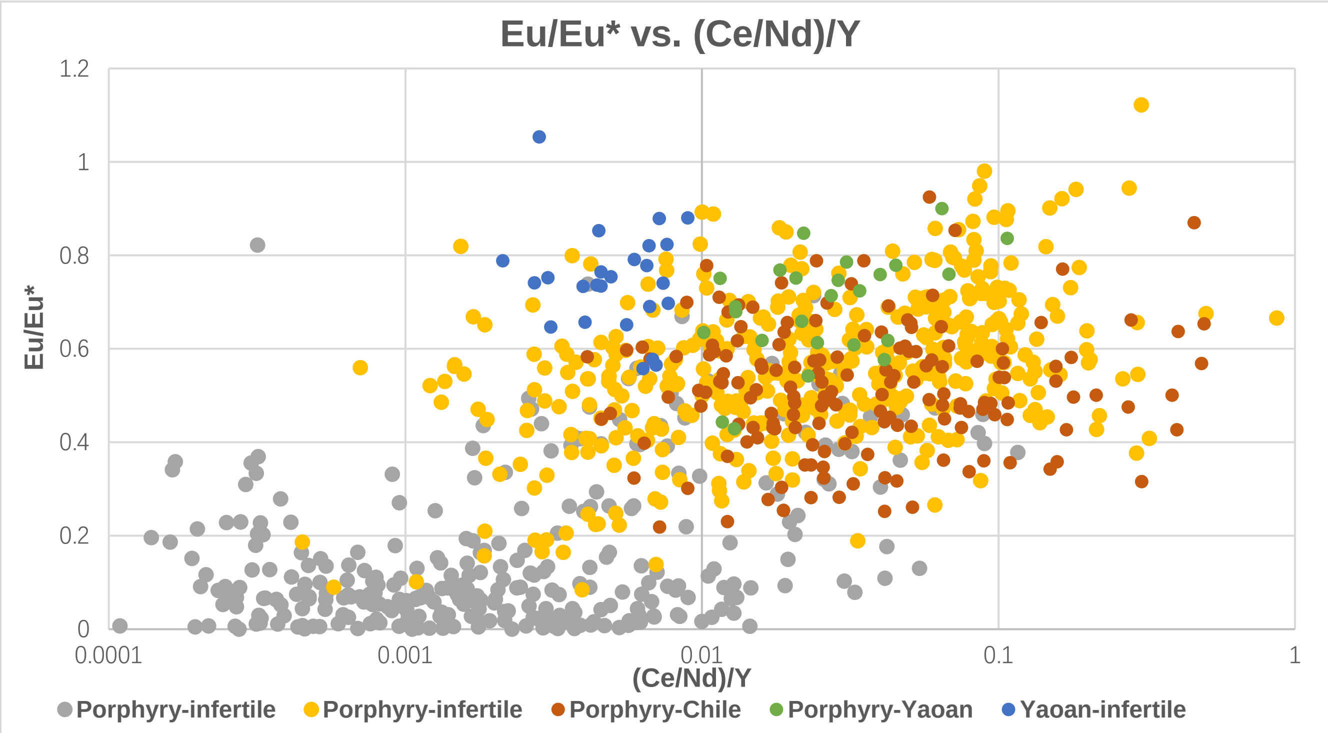


*Figure 8: Zircon Eu/Eu* vs. (Ce/Nd)/Y plot of porphyry suites and infertile suites*

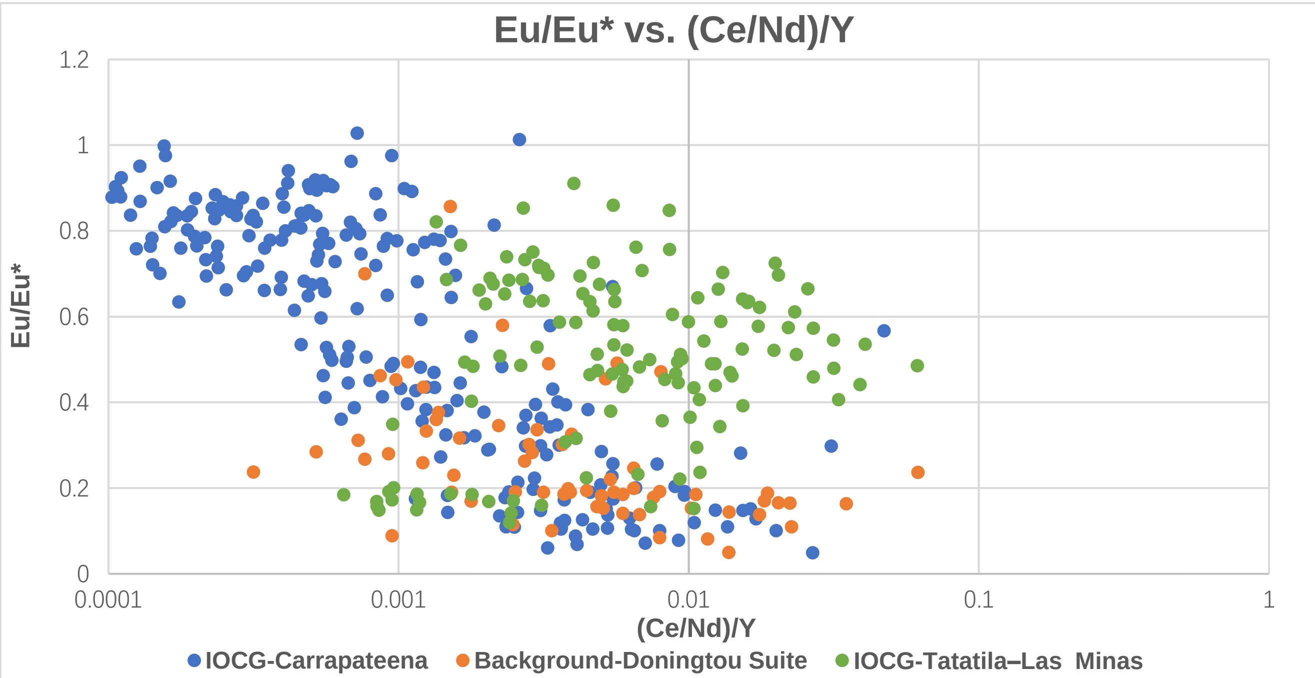


*Figure 9: Zircon Eu/Eu* vs. (Ce/Nd)/Y plot of IOCG suites and infertile suite*

In Figure 8, Zircon Eu/Eu* values (>0.3) and (Ce/Nd)/Y ratios (>0.01) are significantly higher for fertile suites than for Porphyry-infertile, except for Yaoan-infertile.

In Figure 9, most zircons from IOCG deposits have Eu/Eu* > 0.3. For background-Donington Suite, mostly zircon have Eu/Eu* values less than 0.3. Most zircons have (Ce/Nd)/Y less than 0.01.

## 4.6 Plots of 10,000*(Eu/Eu*)/Y vs. (Ce/Nd)/Y

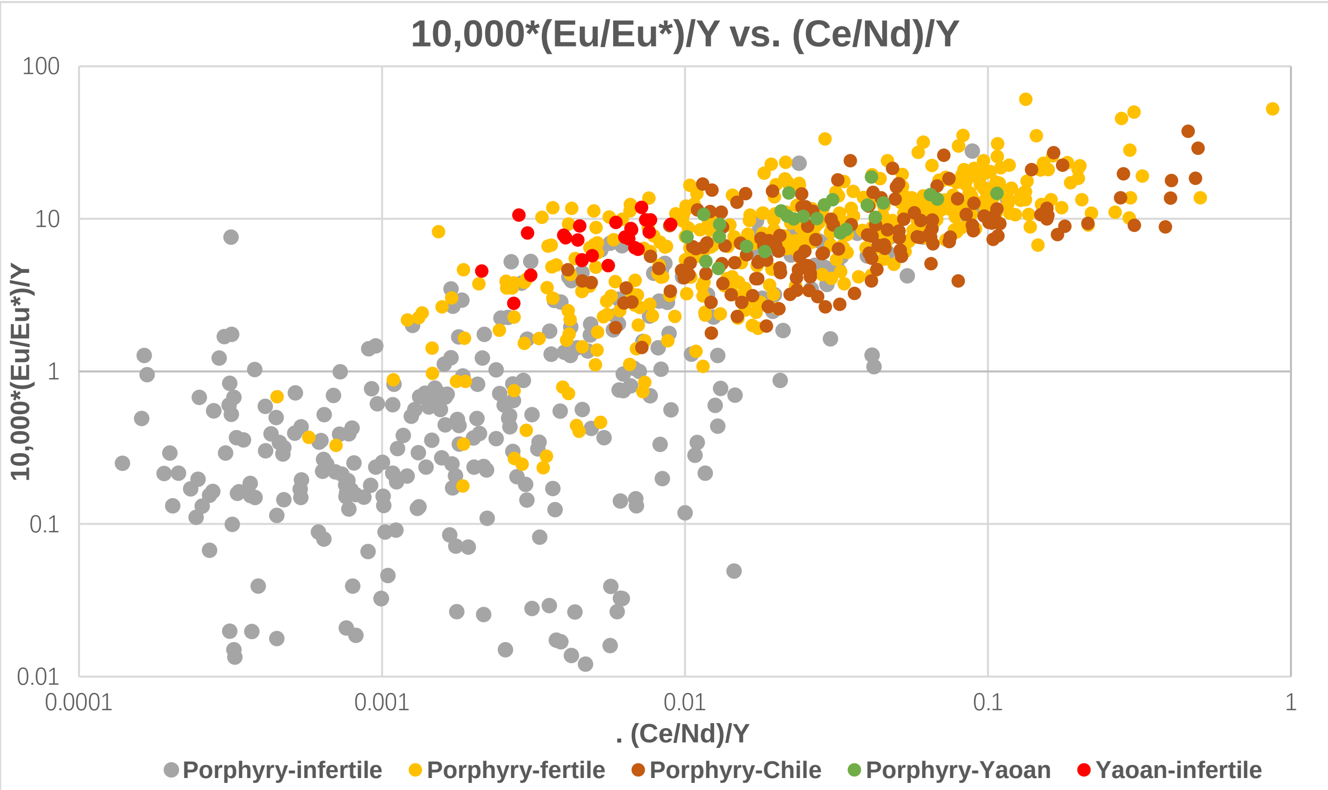


*Figure 10: Zircon 10,000*(Eu/Eu*)/Y vs. (Ce/Nd)/Y plot of porphyry suites and infertile suites*

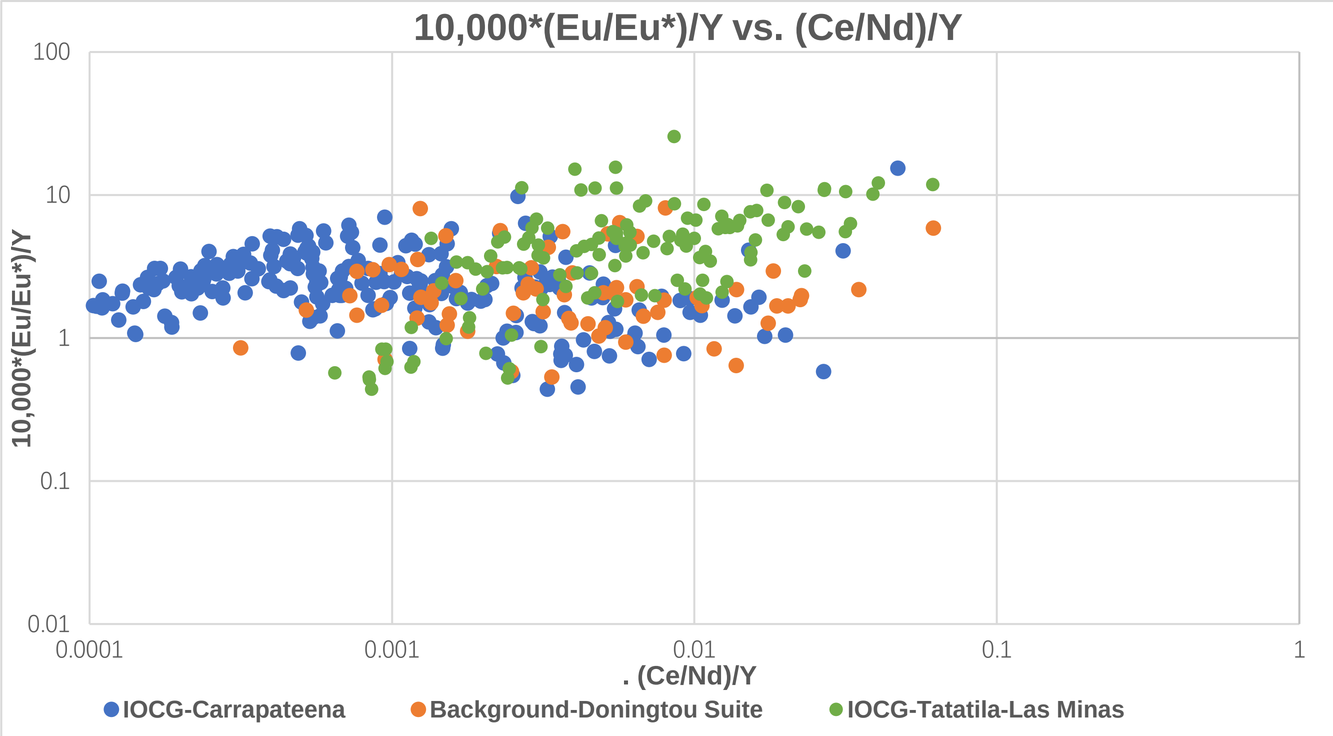


*Figure 11: Zircon 10,000*(Eu/Eu*)/Y vs. (Ce/Nd)/Y plot of IOCG suites and infertile suite*

Figure 10 shows that compared to Porphyry-infertile suites, fertile suites exhibit much higher zircon 10,000*(Eu/Eu*)/Y ratios (>1) and (Ce/Nd)/Y ratios (>0.01).

In figure11, IOCG zircon and background zircon almost overlap together, and all zircon data show 10,000*(Eu/Eu*)/Y ratios (>1).

## 4.7 Plots of Eu/Eu* vs. Dy/Yb

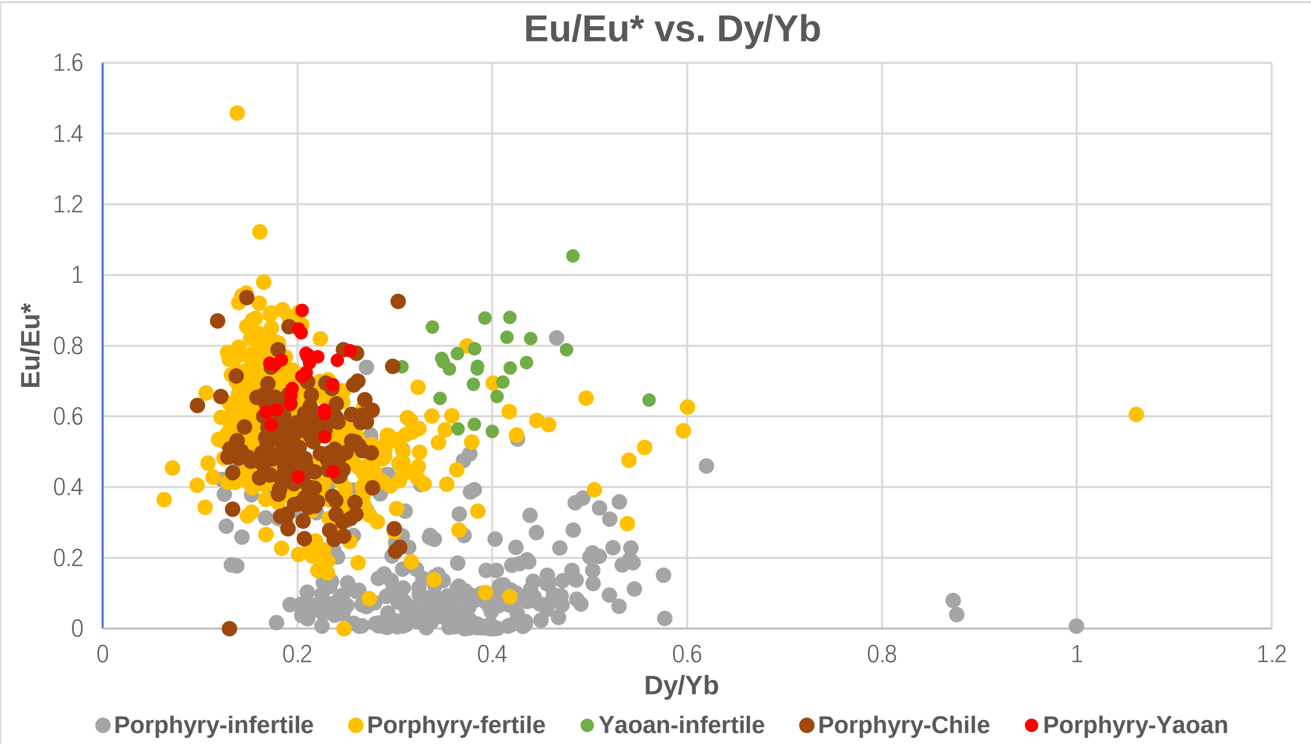


*Figure 12: Zircon Eu/Eu* vs. Dy/Yb plot of porphyry suites and infertile suites*

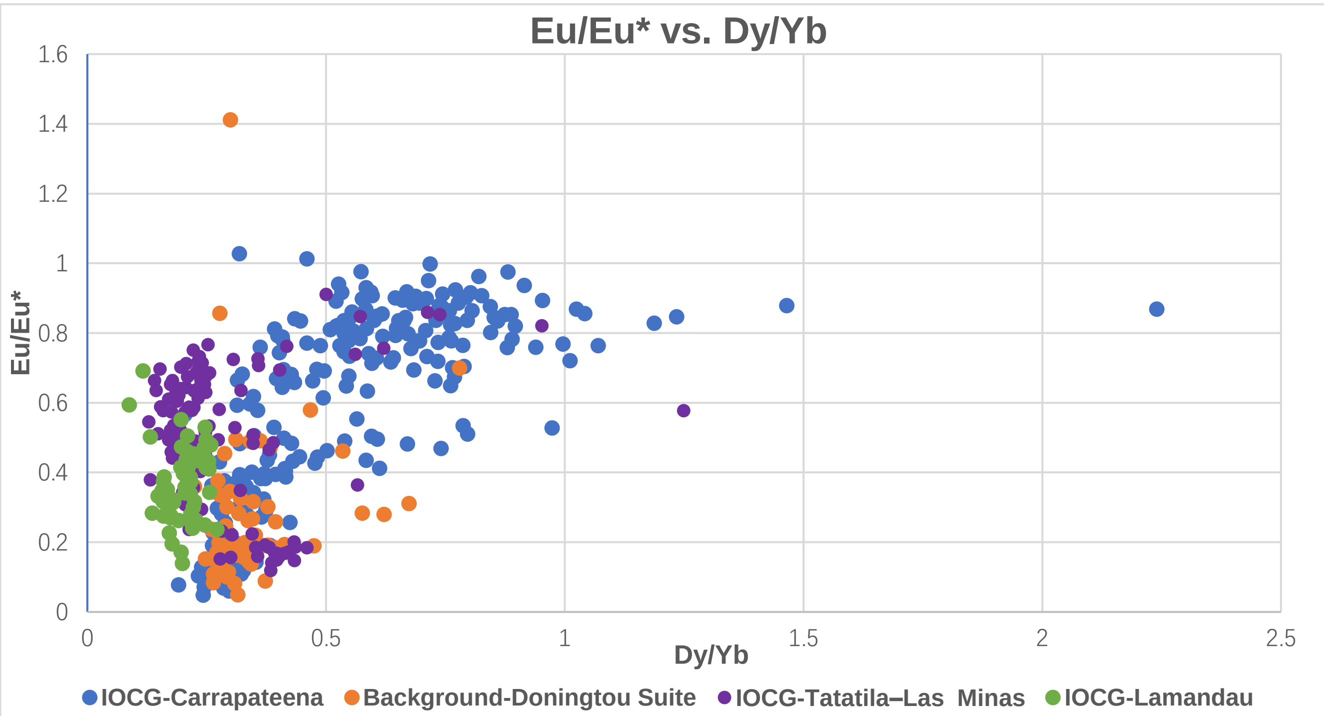


*Figure 13: Zircon Eu/Eu* vs. Dy/Yb plot of IOCG suites and infertile suite*

Figure12 shows porphyry-Yaoan and porphyry-Chile overlap with the porphyry-fertile of Lu et al. (2016). These three porphyry deposits overlap within Eu/Eu* > 0.3 and Dy/Yb < 0.3. The porphyry-infertile is plotted outside these domains - Eu/Eu* < 0.3 and Dy/Yb > 0.3. Porphyry deposits have elevated Eu/Eu* compared to the infertile suites, with the exception of Yaoan-infertile. In addition, Yaoan-infertile does not overlap with the three porphyry deposits nor porphyry-infertile.

Figure13 shows that the IOCG-Tatatila-Las Minas and IOCG-Lamandau do not overlap with the IOCG-Carrapateena, but overlap with the zircons of porphyry mineralisation in figure11.

### 4.8 Plots of Eu/Eu* vs. GdN/YbN

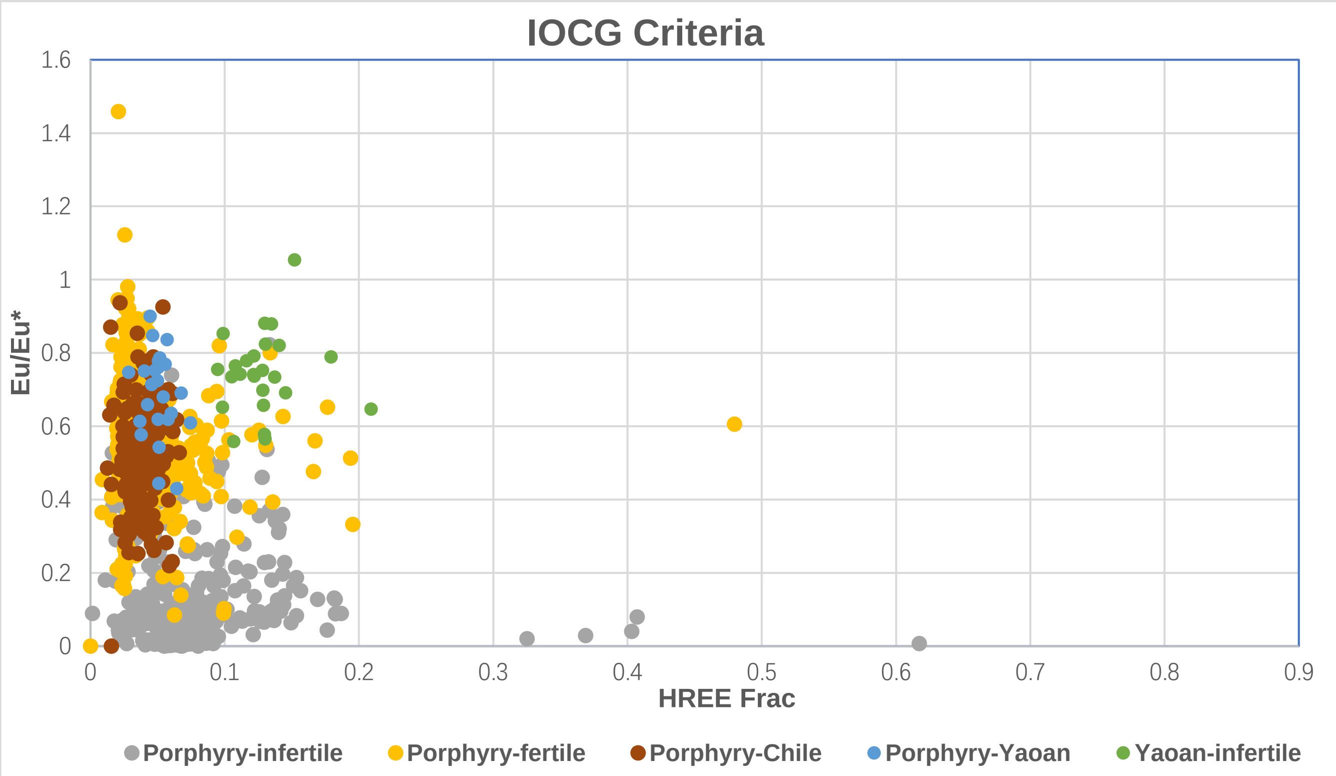


*Figure 14: Zircon Eu/Eu* vs. $Gd_N/Yb_N$ plot of porphyry suites and infertile suites*

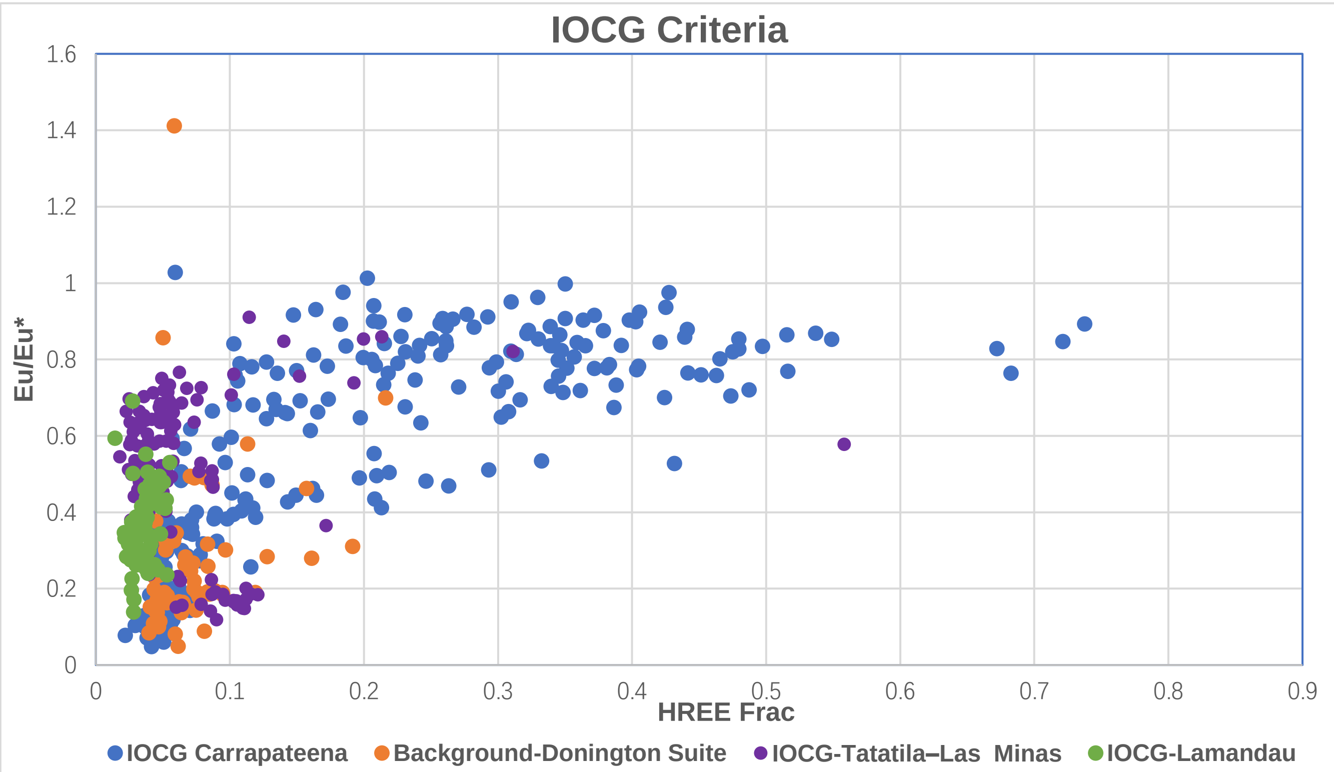


*Figure 15: Zircon Eu/Eu* vs. $Gd_N/Yb_N$ plot of IOCG suites and infertile suite*

Figure14 shows porphyry-Yaoan and porphyry-Chile have a high degree of overlap with porphyry-fertile of Lu et al. (2016) in the ranges of HREE Frac < 0.06, Eu/Eu*(0.25-0.94). Yaoan-infertile has elevated Eu/Eu*and HREE Frac.

Figure15 shows that IOCG-Tatatila-Las Minas and IOCG-Lamandau have a small overlap with IOCG- Carrapateena and Background-Donington Suite and a large overlap with the zircons of porphyry mineralisation in Figure 14.

# 5. DISCUSSION

## 5.1 Previous work

Lu et al. (2016) studied a series of fertile and infertile suites with (LA-ICP-MS) U-Pb age and trace element datasets to elucidate the unique zircon signature diagnostic of parent magmatic mineralisation fertility. Zircon compositions can distinguish between fertile and infertile suites. The best indicators of fertility are zircon Eu/Eu* and (Eu/Eu*)/Y ratios, while zircon (Ce/Nd)/Y and Dy/Yb ratios are moderately useful. In comparison to infertile suites, fertile magmatic suites contain greater zircon Eu/Eu* ratios (>0.3), 10000* (Eu/Eu*)/Y ratios (>1), (Ce/Nd)/Y ratios (>0.01), and lower Dy/Yb ratios ($\leq$0.3). In fertile suites, zircon (Eu/Eu*)/Y ratios are connected positively with (Ce/Nd)/Y ratios, while this correlation is absent in infertile suites (Lu et al., 2016).

Brotodewo et al. (2021) analyzed eight basement material zircon samples from the basement cover unconformity surface from the Gawler Craton, South Australia, four of which directly overlie the IOCG-Carrapateena deposit. The study of Brotodewo et al. (2021) found zircon geochemical signatures characterised by HREE Frac values ($Gd_N/Yb_N \geq 0.15$) and high Eu ratios ($Eu/Eu^* \geq 0.6$). This geochemical signature has been previously identified in zircon derived from the IOCG-Carrapateena orebody and can be used to distinguish zircon associated with IOCG mineralisation from background zircon (Brotodewo et al., 2021).

## 5.2 Eu/Eu* ratio

First of all, Lu et al. (2016) indicate that one of the best indicators of fertility to distinguish mineralised regions is Eu/Eu* ratio > 0.3. The zircon Eu/Eu* ratio > 0.3 in the fertile suites indicates the presence of high-water content or high oxidation state in the main magma, or both (Pizarro et al., 2020; Lu et al., 2016). All zircon samples from the porphyry-Yaoan are > 0.4, and especially the data from the Yaoan-infertile suite are > 0.55. These data conform to the criteria of Lu et al. (2016) that fertile magmas will preserve Eu/Eu* ratio > 0.3. The criterion developed by Brotodewo et al. (2021) for IOCG deposits is the Eu/Eu* ratio > 0.6, double the ratio of porphyry fertility indicators. zircon Eu/Eu* is sensitive to several other parameters such as co-crystalline mineral assemblages, melt composition, and temperature (Nathwani et al., 2021). Therefore, the observed data are more concentrated in the range of 0.4-0.6 and do not exceed 0.6. For the IOCG-Lamandau deposit and the IOCG-Tatatila-Las Minas deposit, the values of median Eu/Eu* are greater than 0.3. However, the IOCG deposits have a very wide range of Eu/Eu* values, so this criterion may only be partially useful.

## 5.3 Eu/Eu* versus Ce/Nd

Figure 6 shows that porphyry zircons are plotted at high Eu/Eu* and a range of Ce/Nd. The wide range of Eu/Eu* and Ce/Nd ratios can be assigned as a general indication of porphyry fertility. Figure 7 shows that the mineralised and non-mineralised zircon of IOCG deposits cannot be clearly distinguished, which means that Eu/Eu* vs Ce/Nd is not suitable for distinguishing zircons from background and borehole zircons that may be associated with mineralisation in IOCG. Ce/Nd ratios for the background and mineralised suites of IOCG deposits overlap between ~3 and 13. Considering that fertile suites are more oxidised than infertile suites, the overlap suggests that Ce/Nd in zircons may not be a good proxy for the melt oxidation state (Lu et al., 2016). Apart from that, zircons from samples from other deposits do show Ce/Nd ratios > 1, suggesting that zircons crystallised from magmas with a high oxidation state (Pizarro et al., 2020). When all the porphyry zircon and IOCG zircon are placed on the same Eu/Eu* vs Ce/Nd plot, there are many overlaps, as shown in the following figure 16, indicating that the plot does not apply to the use of zircon chemistry to distinguish between the two deposit types.

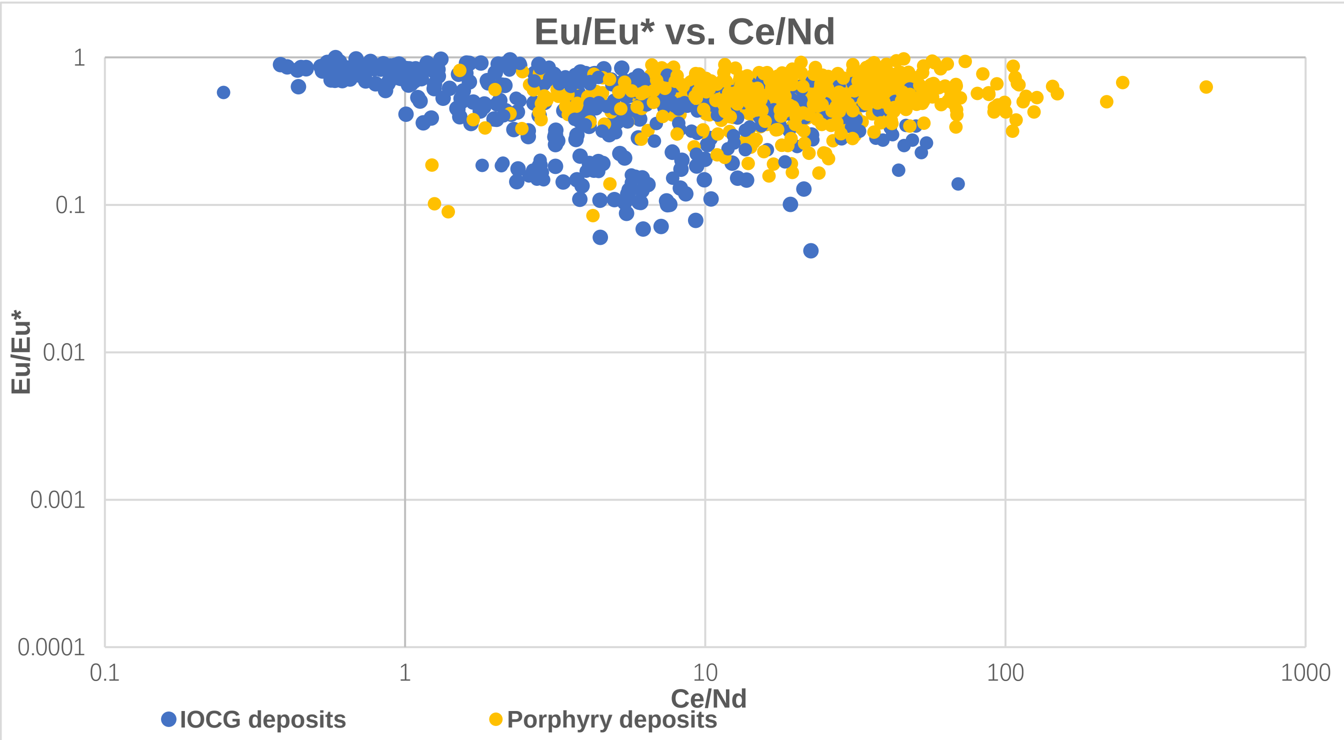


*Figure 16: Zircon Eu/Eu* vs. Ce/Nd plot of IOCG deposits and porphyry deposits*

## 5.4 Eu/Eu* versus (Ce/Nd)/Y

Lu et al. (2016) indicate that the (Ce/Nd)/Y ratio (>0.01) is a moderately effective indicator of fertility. The (Ce/Nd)/Y ratio measured in zircon is associated with high water content in the magma (Lu et al., 2016). For porphyry deposits, Figure 8 is good at distinguishing the difference between data relating to porphyry, infertile zircon, and background zircon. In addition, the (Ce/Nd)/Y ratio was higher (>0.01) in the fertile suites compared to the infertile suites. Zircon with (Ce/Nd)/Y ratios > 0.01 indicate crystallisation from magmas with relatively high-water content (≥4 wt% $H_2O$) (Pizarro et al., 2020). This is because, in water-bearing melts, hornblende crystallizes early in the evolution of the magma and depletes the residual melt in Y (Qu et al., 2021). In addition, when all porphyry zircons are plotted on the same plot, there is a significant difference from porphyry-infertile, although the range of Eu/Eu* and (Ce/Nd)/Y values are exceeded. The Yaoan-infertile does not overlap with the porphyry-infertile nor does it overlap with all the porphyry deposits. In particular, these porphyry zircons are from multiple deposits in different geological regions, which then suggests that the Eu/Eu* vs (Ce/Nd)/Y plot can be used to distinguish between zircon associated with porphyry mineralisation and background zircons from around the world.

For the IOCG deposits, it is difficult to distinguish between the IOCG-Carrapateena, IOCG-Tatatila–Las Minas, and Background-Donington Suite in figure 8, suggesting that it is not a good plot for IOCG exploration using zircon chemistry, although there are some separations between background and IOCG-Carrapateena zircons shown on the Eu/Eu* axis. Figure 17 shows that there is some overlap when porphyry zircon and IOCG zircon are plotted together, but the IOCG zircon is at a lower (Ce/Nd) /Y, indicating that the plot of Eu/Eu* vs. (Ce/Nd)/Y may play a role in distinguishing the two types of deposits.

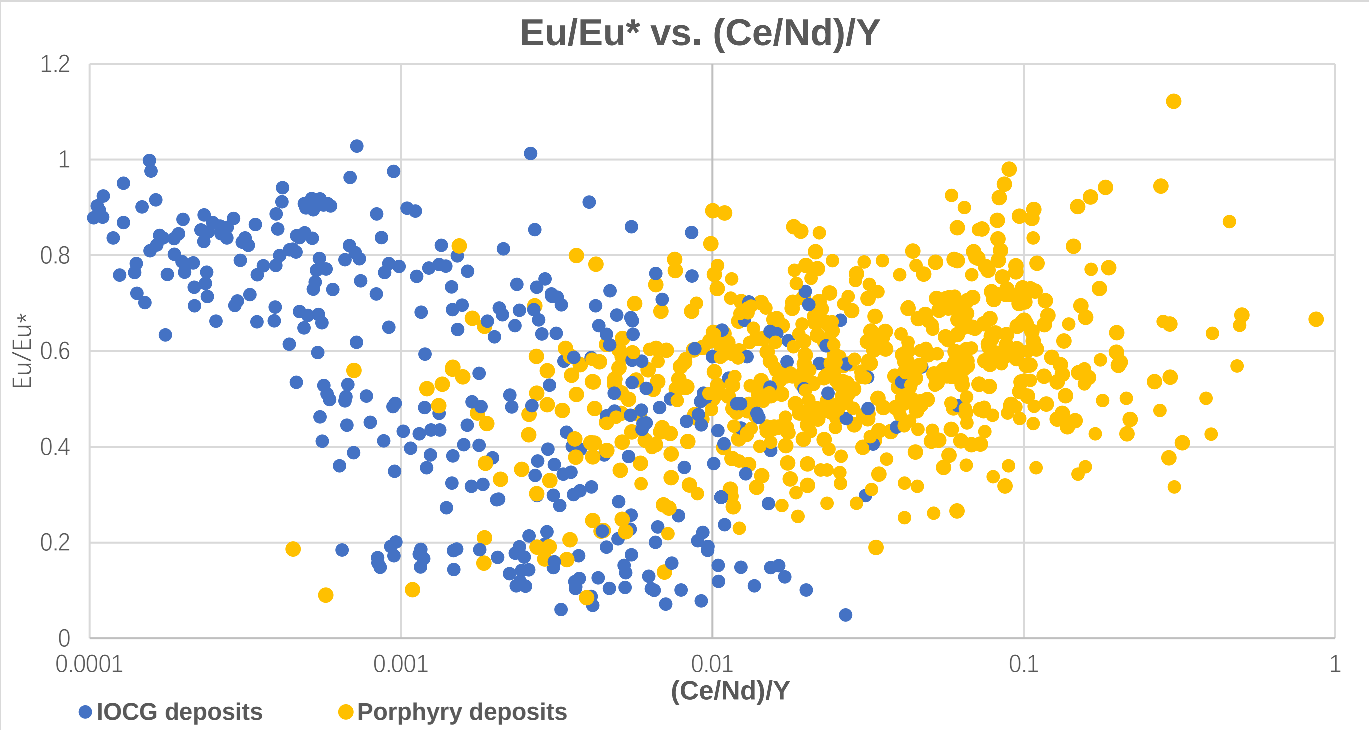


*Figure 17: Zircon Eu/Eu* vs. (Ce/Nd)/Y plot of IOCG deposits and porphyry deposits*

## 5.5 10,000*(Eu/Eu*)/Y versus (Ce/Nd)/Y

Figure 10 shows it is possible to distinguish all the porphyry suites and porphyry-infertile which indicates that this is a good plot for porphyry exploration using zircon chemistry. In the contrast, there are many overlaps between IOCG suites and background (FIg.11), so it can distinguish IOCG zircon and background zircon.

Figure 18 shows that there is some overlap when porphyry and IOCG zircon are plotted together, but the IOCG zircon is at a lower 10,000*(Eu/Eu*)/Y, indicating that the plot of Eu/Eu* vs. 10,000*(Eu/Eu*)/Y may play a role in distinguishing the two types of deposits. In addition, there is some separation between IOCG-Carrapateena and other zircon when porphyry zircon and IOCG zircon are plotted together, so Eu/Eu* vs. 10,000*(Eu/Eu*)/Y plot may be good at distinguishing IOCG-Carrapateena with other deposits.

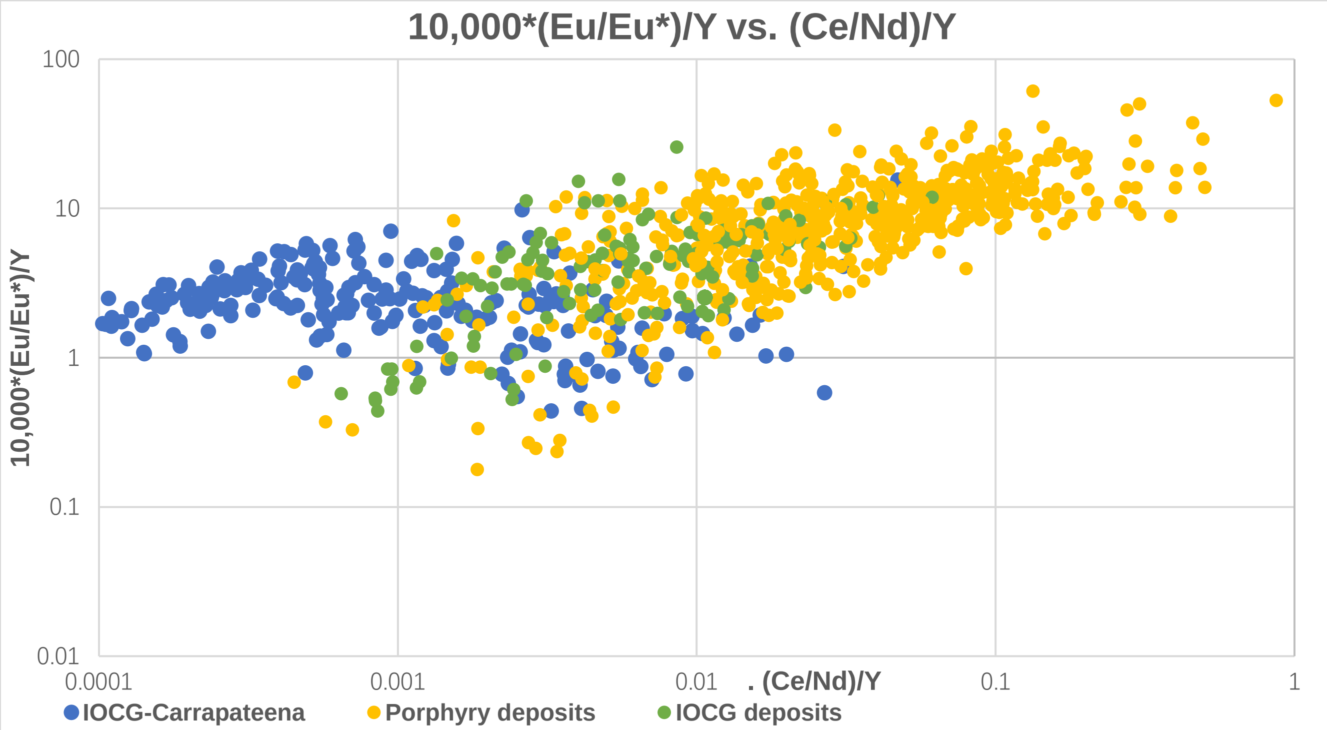


*Figure 18: Zircon Eu/Eu* vs. 10,000*(Eu/Eu*)/Y plot of IOCG deposits and porphyry deposits*

## 5.6 Eu/Eu* versus Dy/Yb

Figure 12 shows that the porphyry-fertile and porphyry-infertile are clearly distinguished. In addition, all the porphyry zircons are plotted together in figure 12, especially since these zircons are from deposits in different regions of the world, indicating that Eu/Eu* vs. Dy/Yb can distinguish background and porphyry zircon. These porphyry zircons are generally less than 0.3, indicating that zircon was formed in magma with HREE content higher than MREE, which can be widely attributed to amphibole fractionation and related to the degree of magmatic fractionation (Pizarro et al., 2020).

Figure 13 shows some separation between background zircon and IOCG zircon. Among them, IOCG-Lamandau and IOCG-Tatatila-Las Minas are clustered together, which are slightly different from the background, but may not be enough to be confident in formulating criteria to distinguish background and

IOCG related. In addition, the difference between IOCG-Carrapateena and background zircon is the largest, indicating that Eu/Eu* vs. Dy/Yb can distinguish IOCG-Carrapateena from background zircon. However, not all IOCG zircon are plotted in the same area, indicating that Dy/Yb does not distinguish them. Therefore, criteria other than Dy/Yb are needed to distinguish zircon from different regions.

## 5.7 Heavy Rare Earth Elements

In figure 14, IOCG-Carrapateena zircon and its background zircon are drawn in completely different regions, which indicates that the chemical composition of IOCG-Carrapateena and background is very different, so this plot is very suitable for distinguishing zircon from deposits similar to Carrapateena style mineralisation. The Background zircon and other IOCG zircon form a vertical trend of zircon from low Eu/Eu* (background) to medium (IOCG-Lamandau) and then to high (IOCG-Tatatila-Las Minas) Eu/Eu*. Eu/Eu* can be used to distinguish these zircons, but HREE Frac does not distinguish them, so criteria other than HREE Frac are required to distinguish zircons in different regions. This indicates the zircon criteria of Brotodewo et al. (2021) the IOCG developed for Gawler Craton may only be used in Gawler Craton, and it also indicates that other criteria need to be developed to distinguish IOCG deposits from other regions.

Zircon for porphyry deposits shows the same vertical trend as the IOCG zircon, almost completely coincident between HREE Frac (0.02-0.06). The background zircons are plotted at the same location as the background Donington zircon, showing that zircon from different regions and unrelated to mineralisation have similar chemical compositions. The $Gd_N/Yb_N$ ratio can be used to reveal the growth order of minerals (Zheng et al., 2021). Eu/Eu* can be combined with $Gd_N/Yb_N$ ratio to track the crystallization of different minerals before or at the same time as zircon crystallization (Lu et al., 2019). Zircon samples from other porphyry zircon and IOCG zircon show loss of intermediate REE (MREE) (i.e., lower $Gd_N/Yb_N$) (Drabon et al., 2021). The overall trend is a typical fractionation trend, which is caused by the crystallization of minerals (e.g., amphibole, sphene, ilmenite, monazite, and apatite) that segregate MREE on HREE and the influence of temperature reduction (Drabon et al., 2021).

# 6. CONCLUSION

In this study, zircon data from six publications were collected and analyzed to evaluate the geochemical criteria established by Lu et al. (2016) and Brotodewo et al. (2021) regarding porphyry copper deposits and IOCG deposits. This study's results show that:

- Eu/Eu* > 0.3 can effectively distinguish zircons from porphyry fertile intrusions and those unrelated to porphyry mineralisation. IOCG-Carrapateena can be distinguished from background zircons by Eu/Eu* > 0.6, however, it is not entirely useful to differentiate IOCG deposits from other regions of the world
- A wide range of Eu/Eu* vs. Ce/Nd can be used as a general indicator of porphyry fertility. Ce/Nd is not suitable for distinguishing zircons from background and borehole zircons that may be related to IOCG mineralisation.
- Although exceeding the range, the Eu/Eu* and (Ce/Nd)/Y values of porphyry deposits diverge considerably from the fertility of porphyry. The plot of (Ce/Nd)/Y may be useful in separating the two types of deposits, however, the IOCG zircon plot is at a low (Ce/Nd)/Y.
- All porphyry suites and infertile suites may be distinguished by 10,000*(Eu/Eu*)/Y vs. (Ce/Nd)/Y, proving that this is a useful plot for porphyry investigation using zircon chemistry.

- HREE Frac can distinguish IOCG-Carrapateena from background zircon very well. More effective indicators are needed to distinguish IOCG deposits in other regions of the world.

Overall, multiple elemental ratios can be used to create criteria for porphyry deposits. However, the criteria developed by Brotodewo et al. (2021) appear to only be applicable in the Gawler Craton, South Australia, as the addition of new datasets from IOCG deposits around the globe showed significant overlap with background samples, showing that the criteria cannot be broadly applied to IOCG systems.

Finally, a number of important limitations need to be considered. Because the number of samples is not enough, there may be some deviation in the results with the input of new datasets. In addition, it is not sufficient whether there are other minerals (such as yttrium phosphate and plagioclase) in the samples that will affect the results. With the development of new technologies, the use of this geochemical exploration tool using zircon may become more standard in exploration, however further work is required to refine the geochemical criteria, particularly for IOCG deposits.

# 7. ACKNOWLEDGMENTS

First and foremost, I would like to express my deep and sincere gratitude to my supervisor Dr. Sudeshna Basugupta for her generous guidance over the past whole year.

I also would like to convey my heartfelt gratitude to my dissertation supervisors Dr. Caroline Tiddy and Dr. Adrienne Brotodewo, for their guidance with the many technical parts of my dissertation and helpful discussions, as well as for their continuous support and endless patience.

In addition, I would like to thank all professors of global natural resource management for their help in the past year and for teaching me valuable knowledge throughout my life.

Finally, I would like to thank my parents for their selfless support of my studies, without whom I would not have the opportunity to study abroad.

Thank you to everyone who has helped me with the dissertation and my best wishes to you all.

# 8. REFERENCE LIST


Alizadeh Sevari, B. and Hezarkhani, A. (2014). Fluid Evolution of the Magmatic Hydrothermal Porphyry Copper Deposit Based on Fluid Inclusion and Stable Isotope Studies at Darrehzar, Iran. *ISRN Geology*, 2014, pp.1–10. doi:10.1155/2014/865941.

American Museum of Natural History. (2019). *Zircon Chronology: Dating the Oldest Material on Earth* | *AMNH*. [online] Available at: https://www.amnh.org/learn-teach/curriculum-collections/earth-inside-and-out/zircon-chronology-dating-the-oldest-material-on-earth.

Bao, Z., Sun, W., Li, C. and Zhao, Z. (2014). U–Pb dating of hydrothermal zircon from the Dongping gold deposit in North China: Constraints on the mineralization processes. *Ore Geology Reviews*, 61, pp.107–119. doi:10.1016/j.oregeorev.2014.02.006.

Brotodewo, A., Tiddy, C., Zivak, D., Fabris, A., Giles, D., Light, S. and Forster, B. (2021). Recognising Mineral Deposits from Cover; A Case Study Using Zircon Chemistry in the Gawler Craton, South Australia. *Minerals*, 11(9), p.916. doi:10.3390/min11090916.

Chiaradia, M. (2020). Gold endowments of porphyry deposits controlled by precipitation efficiency. *Nature Communications*, 11(1). doi:10.1038/s41467-019-14113-1.

Del Real, I., Reich, M., Simon, A.C., Deditius, A., Barra, F., Rodríguez-Mustafa, M.A., Thompson, J.F.H. and Roberts, M.P. (2021). Formation of giant iron oxide-copper-gold deposits by superimposed, episodic hydrothermal pulses. *Communications Earth & Environment*, 2(1). doi:10.1038/s43247-021-00265-w.

Dilles, J.H. and John, D.A. (2021). Porphyry and Epithermal Mineral Deposits. *Encyclopedia of Geology*, pp.847–866. doi:10.1016/b978-0-08-102908-4.00005-9.

Drabon, N., Byerly, B.L., Byerly, G.R., Wooden, J.L., Keller, C.B. and Lowe, D.R. (2021). Heterogeneous Hadean crust with ambient mantle affinity recorded in detrital zircons of the Green Sandstone Bed, South Africa. *Proceedings of the National Academy of Sciences*, [online] 118(8). doi:10.1073/pnas.2004370118.

Encyclopedia Britannica. (2022). *Porphyry copper deposit* | *mineralogy*. [online] Available at: https://www.britannica.com/science/porphyry-copper-deposit.

Forbes, C., Giles, D., Freeman, H., Sawyer, M. and Normington, V. (2015). Glacial dispersion of hydrothermal monazite in the Prominent Hill deposit: An exploration tool. *Journal of Geochemical Exploration*, 156, pp.10–33. doi:10.1016/j.gexplo.2015.04.011.

Fu, B., Page, F.Z., Cavosie, A.J., Fournelle, J., Kita, N.T., Lackey, J.S., Wilde, S.A. and Valley, J.W. (2008). Ti-in-zircon thermometry: applications and limitations. *Contributions to Mineralogy and Petrology*, 156(2), pp.197–215. doi:10.1007/s00410-008-0281-5.

Ghasemi Siani, M., Mehrabi, B., Neubauer, F., Zhang, R. and Cao, S. (2022). Geochronology and geochemistry of zircons from fertile and barren intrusions in the Sangan mining area (NE Iran): Implications for tectonic setting and mineral exploration. *Journal of Asian Earth Sciences*, [online] 233(233), p.105243. doi:10.1016/j.jseaes.2022.105243.

Greenhalgh, K. (2022). *Energy transition to drive doubling of copper demand by 2035: S&P Global*. [online] IHS Markit. Available at:

https://cleanenergynews.ihsmarkit.com/research-analysis/energy-transition-to-drive-doubling-of-copper-demand-by-2035-s.html [Accessed 31 Aug. 2022].

Groves, D.I., Bierlein, F.P., Meinert, L.D. and Hitzman, M.W. (2010). Iron Oxide Copper-Gold (IOCG) Deposits through Earth History: Implications for Origin, Lithospheric Setting, and Distinction from Other Epigenetic Iron Oxide Deposits. *Economic Geology*, 105(3), pp.641–654. doi:10.2113/gsecongeo.105.3.641.

Hazen, R.M. (2010). How Old is Earth, and How Do We Know? *Evolution: Education and Outreach*, [online] 3(2), pp.198–205. doi:10.1007/s12052-010-0226-0.

Hitzman, M.W., Oreskes, N. and Einaudi, M.T. (1992). Geological characteristics and tectonic setting of proterozoic iron oxide (Cu U Au REE) deposits. *Precambrian Research*, 58(1-4), pp.241–287. doi:10.1016/0301-9268(92)90121-4.

Li, H., Watanabe, K. and Yonezu, K. (2014). Zircon morphology, geochronology and trace element geochemistry of the granites from the Huangshaping polymetallic deposit, South China: Implications for the magmatic evolution and mineralization processes. *Ore Geology Reviews*, 60(60), pp.14–35. doi:10.1016/j.oregeorev.2013.12.009.

Li, S., Yang, X. and Sun, W. (2015). The Lamandau IOCG deposit, southwestern Kalimantan Island, Indonesia: Evidence for its formation from geochronology, mineralogy, and petrogenesis of igneous host rocks. *Ore Geology Reviews*, [online] 68, pp.43–58. doi:10.1016/j.oregeorev.2015.01.008.

Liu, H., Liao, R., Zhang, L., Li, C. and Sun, W. (2019). Plate subduction, oxygen fugacity, and mineralization. *Journal of Oceanology and Limnology*, 38(1), pp.64–74. doi:10.1007/s00343-019-8339-y.

Lu, Y.-J., Loucks, R.R., Fiorentini, M., McCuaig, T.C., Evans, N.J., Yang, Z.-M., Hou, Z.-Q., Kirkland, C.L., Parra-Avila, L.A. and Kobussen, A. (2016). Zircon Compositions as a Pathfinder for Porphyry Cu ± Mo ± Au Deposits. *pubs.geoscienceworld.org*, [online] 19(13). doi:10.5382/SP.19.13.

Mojzsis, S.J., Harrison, T.M. and Pidgeon, R.T. (2001). Oxygen-isotope evidence from ancient zircons for liquid water at the Earth's surface 4,300 Myr ago. *Nature*, [online] 409(6817), pp.178–181. doi:10.1038/35051557.

Nathwani, C.L., Simmons, A.T., Large, S.J.E., Wilkinson, J.J., Buret, Y. and Ihlenfeld, C. (2021). From long-lived batholith construction to giant porphyry copper deposit formation: petrological and zircon chemical evolution of the Quellaveco District, Southern Peru. *Contributions to Mineralogy and Petrology*, 176(2). doi:10.1007/s00410-020-01766-1.

Oliveira, C.G. de, Oliveira, F.B. de, Giustina, M.E.S.D., Marques, G.C., Dantas, E.L., Pimentel, M.M. and Buhn, B.M. (2016). The Chapada Cu–Au deposit, Mara Rosa magmatic arc, Central Brazil: Constraints on the metallogenesis of a Neoproterozoic large porphyry-type deposit. *Ore Geology Reviews*, 72(72), pp.1–21. doi:10.1016/j.oregeorev.2015.06.021.

Pizarro, H., Campos, E., Bouzari, F., Rousse, S., Bissig, T., Gregoire, M. and Riquelme, R. (2020). Porphyry indicator zircons (PIZs): Application to exploration of porphyry copper deposits. *Ore Geology Reviews*, 126, p.103771. doi:10.1016/j.oregeorev.2020.103771.

Qu, P., Li, N.-B., Niu, H.-C., Shan, Q., Weng, Q. and Zhao, X.-C. (2021). Difference in the nature of ore-forming magma between the Mesozoic porphyry Cu-Mo and Mo deposits in NE China: Records from apatite and zircon geochemistry. *Ore Geology Reviews*, 135, p.104218. doi:10.1016/j.oregeorev.2021.104218.

Richards, J.P. (2009). Postsubduction porphyry Cu-Au and epithermal Au deposits: Products of remelting of subduction-modified lithosphere. *Geology*, 37(3), pp.247–250. doi:10.1130/g25451a.1.

Roberts, N.M.W., Yang, Q.-Y. and Santosh, M. (2018). Rapid oxygen diffusion during high temperature alteration of zircon. *Scientific Reports*, 8(1). doi:10.1038/s41598-018-22016-2.

Römer, H., Luther, K.-D. . and Assmus, W. (1994). The distribution coefficients of rare earth ions in cubic zirconium dioxide. *Journal of Crystal Growth*, [online] 141(1), pp.159–164. doi:10.1016/0022-0248(94)90107-4.

S&P Global. (2022). *The Future of Copper*. [online] Available at: https://cdn.ihsmarkit.com/www/pdf/0722/The-Future-of-Copper_Full-Report_14July2022.pdf.

Schaltegger, U. (2007). Hydrothermal Zircon. *Elements*, 3(1), pp.51–79. doi:10.2113/gselements.3.1.51.

Schlegel, T.U., Wagner, T. and Fusswinkel, T. (2020). Fluorite as indicator mineral in iron oxide-copper-gold systems: explaining the IOCG deposit diversity. *Chemical Geology*, 548(548), p.119674. doi:10.1016/j.chemgeo.2020.119674.

Sillitoe, R.H. (2010). Porphyry Copper Systems. *Economic Geology*, 105(1), pp.3–41. doi:10.2113/gsecongeo.105.1.3.

Skirrow, R.G. (2021). Iron oxide copper-gold (IOCG) deposits – a review (part 1): settings, mineralogy, ore geochemistry, and classification. *Ore Geology Reviews*, 140, p.104569. doi:10.1016/j.oregeorev.2021.104569.

Spencer, C. (2012). *Zircons*. [online] TravelingGeologist. Available at: http://www.travelinggeologist.com/2012/03/zircons/ [Accessed 1 Sep. 2022].

Stevens, P. (2022). *A coming copper shortage could derail the energy transition, report finds*. [online] CNBC. Available at: https://www.cnbc.com/2022/07/14/copper-is-key-to-electric-vehicles-wind-and-solar-power-were-short-supply.html [Accessed 31 Aug. 2022].

Westhues, A., Hanchar, J.M., Voisey, C.R., Whitehouse, M.J., Rossman, G.R. and Wirth, R. (2017). Tracing the fluid evolution of the Kiruna iron oxide apatite deposits using zircon, monazite, and whole rock trace elements and isotopic studies. *Chemical Geology*, [online] 466(466), pp.303–322. doi:10.1016/j.chemgeo.2017.06.020.

WILLIAMS, P.J. (2001). Australian Proterozoic Iron Oxide-Cu-Au Deposits: An Overview with New Metallogenic and Exploration Data from the Cloncurry District, Northwest Queensland. *Exploration and Mining Geology*, 10(3), pp.191–213. doi:10.2113/0100191.

www.eramet.com. (2020). *All about Zircon* | *Eramet*. [online] Available at: https://www.eramet.com/en/all-about-zircon [Accessed 31 Aug. 2022].

www.zircon-association.org. (2022). *Zircon applications - What is Zircon used for?* | *Zircon Industry Association*. [online] Available at: https://www.zircon-association.org/applications.html.

Yang, W.-B., Niu, H.-C., Shan, Q., Sun, W.-D., Zhang, H., Li, N.-B., Jiang, Y.-H. and Yu, X.-Y. (2013). Geochemistry of magmatic and hydrothermal zircon from the highly evolved Baerzhe alkaline granite: implications for Zr–REE–Nb mineralization. *Mineralium Deposita*, 49(4), pp.451–470. doi:10.1007/s00126-013-0504-1.

Zaman, M. and Antao, S. (2020). Crystal Chemistry and Structural Variations for Zircon Samples from Various Localities. *Minerals*, 10(11), p.947. doi:10.3390/min10110947.

Zheng, Y., Zhang, C., Jia, F., Liu, H. and Yan, Q. (2021). Apatite and Zircon Geochemistry in Yao'an Alkali-Rich Porphyry Gold Deposit, Southwest China: Implications for Petrogenesis and Mineralization. *Minerals*, 11(11), p.1293. doi:10.3390/min11111293.

Zhu, Z. (2016). Gold in iron oxide copper–gold deposits. *Ore Geology Reviews*, 72(1), pp.37–42. doi:10.1016/j.oregeorev.2015.07.001.

# APPENDIX

Click the icon to open Excel